 doi:10.20944/preprints201806.0236.v1

Review

Simulated thermomagnetic properties of $DyAl_2$, $HoAl_2$ and $ErAl_2$ compounds in comparison with the results for $TbAl_2$, $GdAl_2$ and $SmAl_2$ compounds calculated by ATOMIC MATTERS MFA Computation System

R. Michalski[1], J. Zygadło[1,2], T. Lanczewski[3]

[1] Atomic Systems, M. Pszona 41/29, 31-462 Cracow, Poland. rafal.michalski@atomicmatters.eu
[2] Faculty of Mathematics and Computer Science, Jagiellonian University, Łojasiewicza 6, 30-348 Cracow, Poland. jakub.zygadlo@atomicmatters.eu
[3] Atomic Systems, M. Pszona 41/29, 31-462 Cracow, Poland. tomasz.lanczewski@atomicmatters.eu

Abstract: We present the results of calculations of magnetic properties of 3 compounds from Laves phase C15 family: $DyAl_2$, $HoAl_2$ and $ErAl_2$ performed with a new computation system called ATOMIC MATTERS MFA. We compare these results with the recently published results for $TbAl_2$, $GdAl_2$ and $SmAl_2$. The calculation methodology was based on the localized electron approach applied to describe the thermal evolution electronic structure of rare-earth R^{3+} ions over a wide temperature range and to compute magnetocaloric effect (MCE). Thermomagnetic properties were calculated based on the fine electronic structure of $4f^9$, $4f^{10}$ and $4f^{11}$ configurations of the Dy^{3+}, Ho^{3+}, Er^{3+} ions, respectively. Our calculations yield the magnetic moment value and direction; single-crystalline magnetization curves in zero field and external magnetic field applied in various directions of $m(T,\mathbf{B}_{ext})$; the 4f-electronic components of specific heat $c4f(T,\mathbf{B}_{ext})$; and temperature dependence of the magnetic entropy and isothermal entropy change with external magnetic field - $\Delta S(T,\mathbf{B}_{ext})$. The cubic CEF parameter values used for $DyAl_2$ calculations are taken from earlier research of A.L. Lima, A.O. Tsokol and recalculated for universal cubic parameters (A^m_n) for the RAl_2 series. Our studies reveal the importance of multipolar charge interactions when describing thermomagnetic properties of real 4*f* electronic systems and the effectiveness of an applied self-consistent molecular field in calculations for magnetic phase transition simulation.

Keywords: $DyAl_2$, $HoAl_2$, $ErAl_2$, $TbAl_2$, $DyAl_2$, $GdAl_2$,CEF, MFA, MCE, Atomic Matters.

1. Introduction

Condensed matter science research in advanced magnetic refrigerant materials has focused on the giant magnetocaloric effect since its discovery. This has advanced the development of near room-temperature magnetic cooling technology. Understanding and controlling the microscopic quantum mechanisms responsible for storing and releasing material entropy through controlled external magnetic field change processes is one of the biggest challenges in materials science.

The RAl_2 (R = rare earth element) compounds are well known intermetallic materials with interesting magnetic properties at low temperatures. The magnetic properties of this series were studied intensively in the 1970s, but a new wave of interest in this compound family has appeared due to research into materials with a large Magnetocaloric Effect (MCE) for future magnetic refrigerators. We present the results of simulations performed by our ATOMIC MATTERS computation system [1, 2] of thermomagnetic properties of $DyAl_2$. A few calculation results for the $DyAl_2$ compound are compared with experimental data taken from the literature [3-8]. All the lanthanides combine with aluminum to form a RAl_2 compound with the same crystalline structure. This structure is the so-called cubic Laves phase C15 and the point symmetry for the rare earth ion is $\bar{4}3m$.

Preprints (www.preprints.org) | NOT PEER-REVIEWED | Posted: 14 June 2018 doi:10.20944/preprints201806.0236.v1

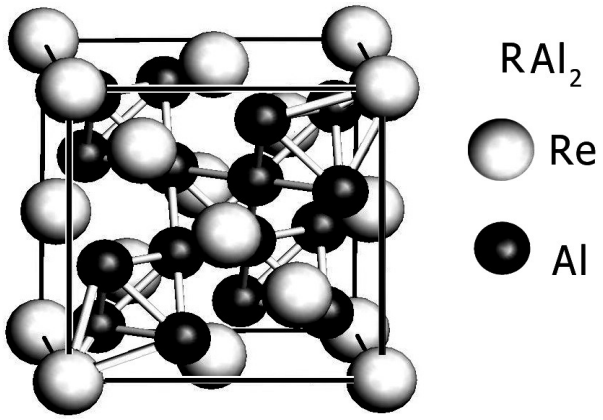

Fig. 1. Cubic elementary cell of RAl_2 Laves phase C15 crystals.

The structure was named after the Swiss crystallographer who performed work on the prototype compound $MgCu_2$. The CEF parameters describing the multipolar charge interaction of R ions in the crystal surrounding in this structure were agreed for both compounds and established by previous studies [3, 4, 9] for $A_4 = +7.164Ka_0$ and $A_6 = -1.038Ka_0$.

2. Computation system

All RAl_2 calculations were performed with ATOMIC MATTERS MFA computation system [2], an extension of the ATOMIC MATTERS application [1] that describes the fine electronic structure and predicts basic magnetic and spectral properties of materials in a paramagnetic state. ATOMIC MATTERS MFA calculates magnetic, calorimetric and spectroscopic properties of atomic-like localized electron systems under the influence of Crystal Electric Field (CEF), spin-orbit coupling, and magnetic interactions, taken both as Mean Field Approximation (MFA) self-consistent, dynamic calculations and the influence of established external magnetic fields B_{ext} [2]. ATOMIC MATTERS MFA calculates macroscopic properties of materials in defined temperature regions, especially around phase transition temperature, such as: magnetic moment $m(T,\mathbf{B}_{ext})$ (spin and orbital, directional components); localized electron specific heat $c_{4f}(T,\mathbf{B}_{ext})$; localized electron entropy with a useful tool-set for MCE; isothermal entropy change $-\Delta S(T,\mathbf{B}_{ext})$ calculations; evolution of energy level positions; total free energy.

Both calculation systems contain advanced Graphic User Interface (GUI) with a system of hierarchical tabs for calculation results management, 3D interactive visualizations of potentials and fields based on Open GL graphic engine, tools and databases for convenient and effective work. More in-date information about Atomic Matters computation systems is available on our web page [10].

3. Theoretical background

The theoretical approach applied at the heart of ATOMIC MATTERS MFA computation system is deeply rooted in atomic physics. Taking into consideration the individual population of states of the fine electronic structure of ions/atoms at different temperatures according to Boltzmann statistics make it possible to define the temperature dependencies of single ionic properties. ATOMIC MATTERS MFA can simulate phase transitions of ionic/atomic systems according to dynamic calculations of the molecular field $\mathbf{B}_{mol}$, simply defined as:

$$\mathbf{B}_{mol}(T) = n_{mol}\,\mathbf{m}(T) \tag{1}$$

This interacts with ions to induce their magnetic moments. Such self-consistent calculations can only be performed after establishing the molecular field factor n_{mol} that is closely related to the temperature of phase transitions T_C.

Preprints (www.preprints.org) | NOT PEER-REVIEWED | Posted: 14 June 2018 doi:10.20944/preprints201806.0236.v1

For rapid calculations in a thermodynamically stable temperature region, ATOMIC MATTERS offers the following CEF + Spin-Orbit + Zeeman Hamiltonian according to the chosen calculation space of ground multiplet $|J,J_z\rangle$ or ground atomic term $|L,S,L_z,S_z\rangle$, respectively [1]:

$$H_J = H_{CEF} + H_{Zeeman} = \sum_n \sum_m B_n^m \hat{\mathbf{O}}_n^m(J, J_z) + g_L \mu_B \mathbf{J} \cdot \mathbf{B}_{ext} \quad (2)$$

or

$$H_{LS} = H_{CEF} + H_{S\text{-}O} + H_{Zeeman} = \sum_n \sum_m B_n^m \hat{\mathbf{O}}_n^m(L, L_z) + \lambda \mathbf{L} \cdot \mathbf{S} + \mu_B (\mathbf{L} + g_e \mathbf{S}) \cdot \mathbf{B}_{ext} \quad (3)$$

For all Hamiltonians: B^m_n denotes CEF parameters, $\mathbf{O}^m_n$ are Stevens operators, λ is the spin-orbit constant, and g_L and $g_e \approx 2.002319$ are the gyromagnetic factors of a whole ion or single electron, respectively. For a whole ion or electron respectively, μ_B is the Bohr magneton and $\mathbf{B}_{ext}$ is the external magnetic field. In all cases, calculations in the $|L,S,L_z,S_z\rangle$ space are more physically appropriate due to their completeness, but traditional calculations with base $|J,J_z\rangle$ can also be performed by our computation systems for comparisons and rapid estimations [2]. For calculating properties in temperatures around the magnetic phase transition point, a self-consistent methodology for molecular field calculation called Mean Field Approximations (MFA) is applied. The idea behind this method is the estimation of direction and value of the magnetic field (molecular field) generated by ions at a defined temperature, and calculation of the influence of this magnetic field for electronic state structures of ions. In a selected calculation space, according to (1) we define a molecular field as an expected value of the total moment of the 4f electronic subshell multiplied by the molecular field, inter ionic exchange factor n_{mol}:

$$\mathbf{B}_{mol} = -n_{mol}\, g_L \mu_B \langle \mathbf{J} \rangle \quad (4)$$

or

$$\mathbf{B}_{mol} = -n_{mol}\, \mu_B \langle \mathbf{L} + g_e \mathbf{S} \rangle \quad (5)$$

where g_L and $g_e \approx 2.002319$ are gyromagnetic factors. On the basis of the calculated electronic level structure $E_i(T)$, the directional components of magnetic moments are established for all identical ions. This means that Hamiltonian matrix diagonalization is performed for all defined temperature steps recurrently, in contrast to simple ATOMIC MATTERS calculations [1], which diagonalize matrices one time for a single run and deduce all thermodynamic properties from the stable discrete energy level structure obtained. This self-consistent procedure provides temperature-dependent energy level structure and has one only free parameter, n_{mol}, called the molecular field parameter. The value of n_{mol} is closely related to the phase transition temperature T_C of the macroscopic structure of ions. The formal expression of the full Hamiltonian used by ATOMIC MATTERS MFA computation system, according to the chosen calculation space $|J,J_z\rangle$ or $|L,S,L_z,S_z\rangle$, respectively, has the form:

$$H_{J\,mol} = H_J + H_{\mathrm{mol}} = +\sum_n \sum_m B_n^m \hat{\mathbf{O}}_n^m(J, J_z) + n_{mol}\, g_L^2\, \mu_B^2 \left(-\mathbf{J} \langle \mathbf{J} \rangle + \frac{1}{2} \langle \mathbf{J} \rangle^2 \right) + g_L \mu_B \mathbf{J} \cdot \mathbf{B}_{ext} \quad (6)$$

or

$$H_{LS\,mol} = \sum_n \sum_m B_n^m \hat{\mathbf{O}}_n^m(L, L_z) + \lambda \mathbf{L} \cdot \mathbf{S} + n_{mol}\, \mu_B^2 \left(-(\mathbf{L} + g_e \mathbf{S}) \langle \mathbf{L} + g_e \mathbf{S} \rangle + \frac{1}{2} \langle \mathbf{L} + g_e \mathbf{S} \rangle^2 \right) + \mu_B (\mathbf{L} + g_e \mathbf{S}) \cdot \mathbf{B}_{ext} \quad (7)$$

The eigenvectors of the Hamiltonian are described according to the selected calculation base by the total momentum quantum numbers $|J,J_z\rangle$ or spin and orbit quantum numbers $|L,S,L_z,S_z\rangle$. Using the commutation relations of the angular momentum operators, we obtain information about expected values of the projections of the magnetic momentum of all electronic states at chosen temperature [2]:

$$m_J^{\alpha}(T) = \frac{g_L \mu_B}{Z(T)} \sum_i \langle J_\alpha^i \rangle \exp\left(-\frac{E_i(T)}{k_B T} \right) \quad (8)$$

Preprints (www.preprints.org) | NOT PEER-REVIEWED | Posted: 14 June 2018 doi:10.20944/preprints201806.0236.v1

$$m_{LS}^{\alpha}(T) = \frac{\mu_B}{Z(T)} \sum_i < L_\alpha^i + g_e S_\alpha^i > \exp\left(-\frac{E_i(T)}{k_B T}\right) \quad (9)$$

where: α indexes directional components, i – numbers the Hamiltonian eigenstates, while Γi represents the expected value of the total angular momentum along the α-axis in the i-th state:

$$<J^i_\alpha> = <\Gamma_i(T)\,|\,\mathbf{J}_\alpha\,|\,\Gamma_i(T)> \quad (10)$$

$$<L^i_\alpha + g_e S^i_\alpha> = <\Gamma_i(T)\,|\,\mathbf{L}^i_\alpha + g_e \mathbf{S}^i_\alpha\,|\,\Gamma_i(T)> \quad (11)$$

All property calculations can be done for 3D (x,y,z) real space by using complex Hamiltonian matrix elements defined by full expressions of extended Stevens $\mathbf{O}^m_n$ operators [11]. Mostly for comparison with traditional calculation results, ATOMIC MATTERS also offers a 2D (x,z) calculation methodology of a simplified model of CEF interactions defined by Stevens $\mathbf{O}^m_n$ operators with real number matrix elements only [12].

Taking into consideration the possibility of the thermal population of states, we automatically obtain the thermal evolution of single ion properties of the whole compound [13, 14].

Under the thermodynamic principle at temperature T = 0K only the ground state is occupied. In this situation, the magnetic moment of the ion is exactly equal to the momentum of the ground state. If the temperature rises, the probability of occupying higher states increases according to Boltzmann statistics. The number of ions with energy E_i within a system at temperature T is:

$$N_i(T) = N_0 \frac{exp\left(-\frac{E_i(T)}{k_B T}\right)}{Z(T)} \quad (12)$$

where $N_0 \approx 6.022 \cdot 10^{23}$ mol^{-1} (Avogadro constant) and Z(T) is the sum of states. Knowing the sum of the states, we can determine the Helmholtz free energy F(T):

$$F(T) = -k_B T \ln Z(T) \quad (13)$$

According to thermodynamic principles, the contribution of localized electrons to the total specific heat of materials can be calculated by numerical derivation of Helmholtz free energy:

$$c_{mol}(T) = -T\left(\frac{\partial^2 F(T)}{\partial T^2}\right) \quad (14)$$

This makes it possible to calculate entropy according to the well-known definition:

$$S(T) = S(0) + \int_0^T \frac{c(T)}{T} dT \quad (15)$$

The value of electronic entropy for a defined temperature is difficult to compare, but the isothermal change of the entropy of the system at given temperature is a very important material parameter that describes its thermomagnetic properties. Isothermal entropy change -ΔS(T,$\mathbf{B}_{ext}$), captured for different temperatures under the influence of different magnetic fields, is one the most important properties of a material that describes its usefulness as a magnetocaloric material. The value -ΔS(T,$\mathbf{B}_{ext}$), which was extracted from experimental specific heat measurements, is often presented as a basic description of the magnetocaloric effect (MCE) of materials [3-7]. In our approach, isothermal entropy change can be directly calculated from (15) according to the definition:

$$\Delta S(T,\mathbf{B}_{ext}), = S(T,\mathbf{B}_{ext}=0) - S(T,\mathbf{B}_{ext}). \quad (16)$$

ATOMIC MATTERS MFA also provides single-ionic magnetocrystalline anisotropy calculations that include full calculations (without Brillouin function approximation) of $K_i(T)$ magnetocrystalline constants for defined temperature ranges according to the relations [15]:

Preprints (www.preprints.org) | NOT PEER-REVIEWED | Posted: 14 June 2018 doi:10.20944/preprints201806.0236.v1

$$K_1(T) = \frac{3}{2}B_2^0\left(\left\langle \hat{\mathbf{O}}_2^0\right\rangle - \left\langle \hat{\mathbf{O}}_2^2\right\rangle\right) - 5B_4^0\left(\left\langle \hat{\mathbf{O}}_4^0\right\rangle - 3\left\langle \hat{\mathbf{O}}_4^2\right\rangle\right) - \frac{21}{2}B_6^0\left(\left\langle \hat{\mathbf{O}}_6^0\right\rangle - 5\left\langle \hat{\mathbf{O}}_6^2\right\rangle\right),$$
$$K_2(T) = \frac{35}{8}B_4^0\left(\left\langle \hat{\mathbf{O}}_4^0\right\rangle - 4\left\langle \hat{\mathbf{O}}_4^2\right\rangle + \left\langle \hat{\mathbf{O}}_4^4\right\rangle\right) + \frac{63}{8}B_6^0\left(\left\langle \hat{\mathbf{O}}_6^0\right\rangle - 20\left\langle \hat{\mathbf{O}}_6^2\right\rangle + 5\left\langle \hat{\mathbf{O}}_6^4\right\rangle\right), \quad (17)$$
$$K_2^*(T) = \frac{1}{8}\left(B_4^0\left\langle \hat{\mathbf{O}}_4^0\right\rangle + 5B_6^4\left\langle \hat{\mathbf{O}}_6^4\right\rangle\right), \quad {}_3(T) = -\frac{231}{16}B_6^0\left\langle \hat{\mathbf{O}}_6^0\right\rangle, \quad K_3^*(T) = -\frac{11}{16}B_6^4\left\langle \hat{\mathbf{O}}_6^4\right\rangle.$$

where: $\left\langle \hat{\mathbf{O}}_n^m\right\rangle$ denotes thermal expected values of Stevens operators we defined according to C. Rudowicz [11]. The exchange interactions simulated according to MFA methodology defined by (1) provide simulated properties strongly dependent on only one parameter, n_{mol}, which is closely related to the temperature of phase transitions T_C. It is easy to find the value of n_{mol} for correct T_C, but the value of this parameter can be estimated according to De Gennes scaling [16]:

$$T_C \sim G(f^n),\ G(f^n)=(g_L-1)^2J(J+1) \quad (18)$$

De Gennes scaling is also a useful tool for n_{mol} estimation, as charge surroundings can be transferred between ions in series. The CEF part of Hamiltonian contains Stevens CEF parameters B^m_n. The values of these parameters are only appropriate for a defined ion. The recalculation of B^m_n parameters defined for an ion A in the crystal lattice surrounding of ion B in the same crystalline position follows the simple scheme:

$$B^m_n \text{ (ion A)} \rightarrow A^m_n \rightarrow B^m_n \text{ (ion B)} \quad (19)$$

Stevens B^m_n parameters can be expressed by universal A^m_n parameters, according to the calculation space used, as follows:

$$|J,J_z\rangle;\ B^m_n(J,J_z)=\theta_n(J)\langle r_{4f}{}^n\rangle A^m_n$$
$$|L,S,S_z,L_z\rangle;\ B^m_n(L,L_z)=\theta_n(L)\langle r_{4f}{}^n\rangle A^m_n \quad (20)$$

where values of 2, 4, 6–th power of the average radius of 4f shell $\langle r^n\rangle$ have been calculated by many authors using the Hartree-Fock-type methodology, and the results can be easily found in the literature. The θ_n parameters are the J- or L-dependent Clebsh-Gordan-type factors, sometimes called α,β,γ-Stevens factors $\theta_2=\alpha$, $\theta_4=\beta$, $\theta_6=\gamma$, which can be expressed by finite equations available in [17, 18]. The values of $\langle r_{4f}{}^n\rangle$ are stored in the open database of the system together with a reference. In all calculations, we used the $\langle r_{4f}{}^n\rangle$ values tabulated in [18]. The ability to recalculate CEF parameters between ions and calculation spaces offers a unique chance to establish an acceptable simplification of methodology. The recalculation of CEF parameters in Atomic Matters systems is fully automated, but an explicit Stevens Factors Calculator is also available.

4. Calculation results for $DyAl_2$

The CEF parameters used for $DyAl_2$ were originally estimated by H.G. Purwins and A. Leson [4] and cited by A.L. Lima et al. [3].

The local symmetry of coordinating charges of R^{3+} ions defines number of non-zero CEF parameters. In case of cubic crystal field, there are only two non-zero CEF parameters describing the coordinating potential. The relation between cubic CEF parameters B_4 and B_6 and generally defined CEF parameters used in Hamiltonians (2), (3), (6) and (7) is simple:

$$B_4 = B_4^0 = 5B_4^0,\ B_6 = B_6^0 = -21B_6^4 \quad (21)$$

The parameters were provided in cubic Stevens notation: $B_4 = -(5.5\pm1.2)\cdot10^{-5}$ meV and $B_6 = -(5.6\pm0.8)\cdot10^{-7}$ meV. We recalculated the values of Stevens parameters to obtain universal, ion-independent CEF notation A^m_n according to (19) and (20). The parameters A_4 = +7.164Ka$_0$ and A_6 = -1.038Ka$_0$ obtained in this manner define charge surroundings of R ion in a crystal lattice of RAl_2. The visualization of this potential is shown in Fig. 2. The triangular shapes that are connected to the location of the coordinating Al ions are located symmetrically in cubic surroundings and reflect the atom position in the elementary cell of Laves phase shown in Fig. 1.

Preprints (www.preprints.org) | NOT PEER-REVIEWED | Posted: 14 June 2018 doi:10.20944/preprints201806.0236.v1

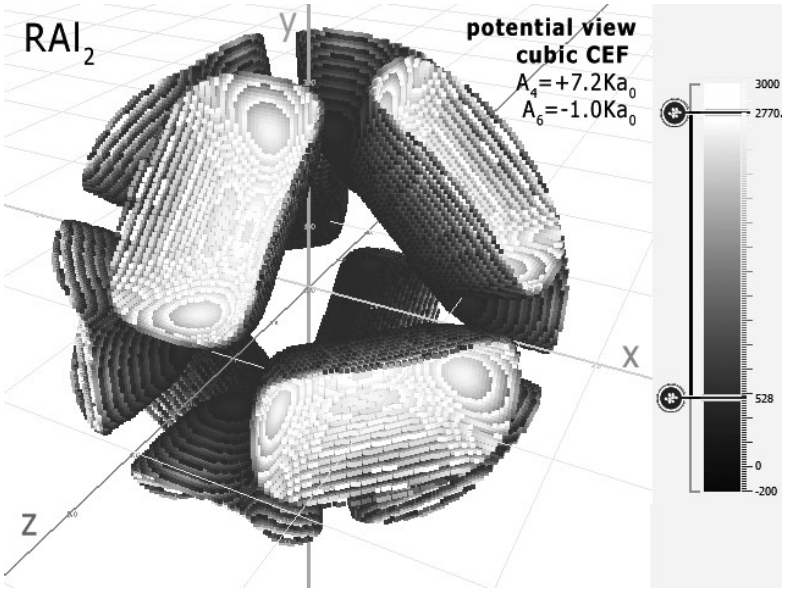

Fig. 2. Crystal Field potential visualization of cubic surrounding of R-ions in RAl_2 defined by CEF parameters: $A_4 = +7.164Ka_0$ and $A_6 = -1.038Ka_0$. The visualization of positive sign potential is cut off by the sphere.

The intermetallic compound $DyAl_2$ has strong magnetocaloric properties at low temperatures. This compound has been extensively studied both theoretically and experimentally [3-6].

In this section, we present the results of an investigation of the magnetic and magnetocaloric properties of a $DyAl_2$ single crystal. We have attributed the magnetism of $DyAl_2$ to the Dy^{3+} ions and calculated the fine electronic structure of the $4f^9$ electronic system in cubic symmetry taking into account the crystal field and inter-site, spin-dependent exchange interactions. The energy level scheme derived is associated with the reduction of the degeneracy of the lowest atomic term ^6H given by Hund's first two rules.

The full calculated energy level structure in the $|L,S,L_z,S_z\rangle$ calculation space is shown in Fig. 3. The obtained overall splitting is strongly dependent on the strength of spin-orbit intra-atomic interactions. We use the free-ion value of the spin-orbit constant of Ho^{3+} ions $\lambda = -550K$ and obtain an overall splitting of ^6H atomic term of about 15000K = 1.3 eV. Details of ground states structure are shown in Fig. 4.

Preprints (www.preprints.org) | NOT PEER-REVIEWED | Posted: 14 June 2018 doi:10.20944/preprints201806.0236.v1

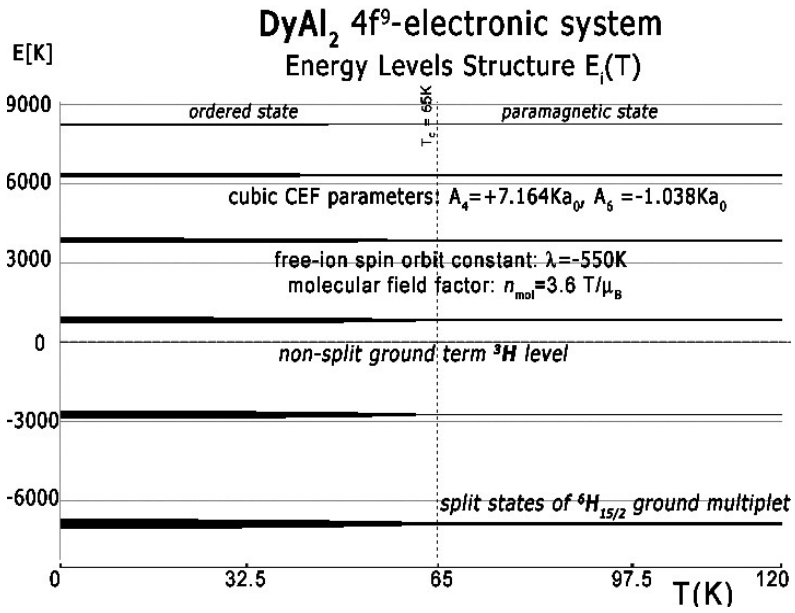

Fig. 3. The result of calculation of energy level position vs. temperature of the fine electronic structure of $4d^9$ electronic configuration of Dy ions in $DyAl_2$ in $|L,S,L_z,S_z>$ space under the influence of intra-atomic spin-orbit coupling, inter-atomic self-consistent molecular magnetic field and Crystal Electric Field (CEF).

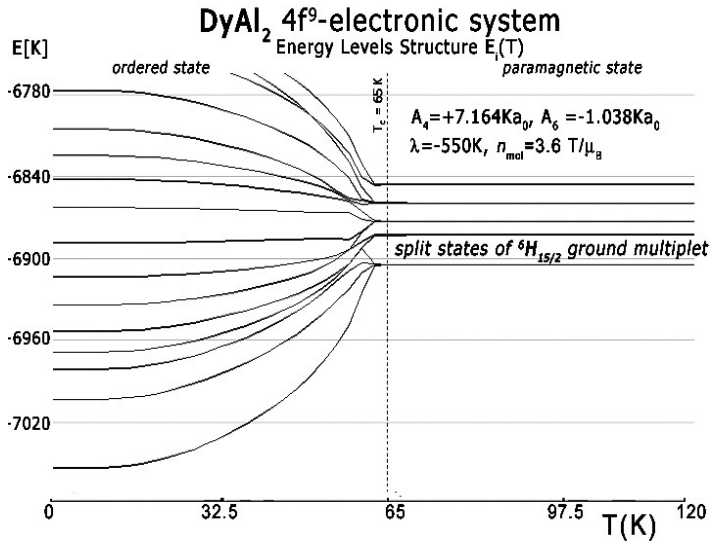

Fig. 4. Ground multiplet energy level structure vs. temperature calculated for $4f^9$ electronic system of Dy ions in $DyAl_2$. At Curie temperature $T_C = 65K$ the structure splits under the influence of molecular field and CEF.

In the absence of an external magnetic field, the induced molecular field splits and moves into degenerated states. The value of the molecular field factor established for $DyAl_2$, which reproduces T_C well at about 63K, is $n_{mol} = 3.6T/\mu_B$. Above T_C, the material is in a paramagnetic state and the ground state of Dy ions is degenerated. The ground quartet consists of two quasi-doublets. The wave functions of the ground paramagnetic state of Dy ions in $DyAl_2$ can be expressed in $|J_z>$ notation:

Preprints (www.preprints.org) | NOT PEER-REVIEWED | Posted: 14 June 2018 doi:10.20944/preprints201806.0236.v1

$$\Gamma_1=-0.137|-5.5\rangle+0.619|-1.5\rangle+0.723|2.5\rangle-0.275|6.5\rangle$$
$$\Gamma_1'=-0.137|5.5\rangle+0.619|1.5\rangle+0.723|-2.5\rangle-0.275|-6.5\rangle$$
$$\Gamma_2=+0.730|-7.5\rangle-0.612|-3.5\rangle-0.303|0.5\rangle-0.026|4.5\rangle$$
$$\Gamma_2'=+0.730|7.5\rangle-0.612|3.5\rangle-0.303|-0.5\rangle-0.026|-4.5\rangle \quad (22)$$

The molecular field splits these states at $T < T_C$. The value of the molecular field changes and at $T = 0$ (absolute zero) $B_{mol} = 23.6$ T and its direction is along the [100] crystal direction, which is the x-axis in our CEF potential picture from Fig. 2. In this condition, the wave function of the ground singlet gets the form:

$$\Gamma_0=0.988|-7.5\rangle-0.153|-3.5\rangle-0.011|0.5\rangle-0.0001|4.5\rangle \quad (23)$$

The influence of the external magnetic field applied along different crystal directions for the structure of the lowest electronic states is shown in Fig. 5 and Fig. 6. The comparison between the effects of the external magnetic field applied along different directions reveals the appearance of an anomaly in the level structure if an external field is applied along the [110] crystal direction. This anomaly corresponds to the specific heat curve from Fig. 7, computed in the same external field direction. The specific heat of $DyAl_2$ (spec. heat of $4f^9$ electronic system +Debye crystal lattice component) shown in Fig. 7 was calculated for the same external field conditions as experimental measurements from [3]. Excellent agreement between calculated specific heat and experimental data is also confirmed if the external magnetic field is applied along the [100] direction. The results of this calculation and reference measurements from [3] are shown in Fig. 8.

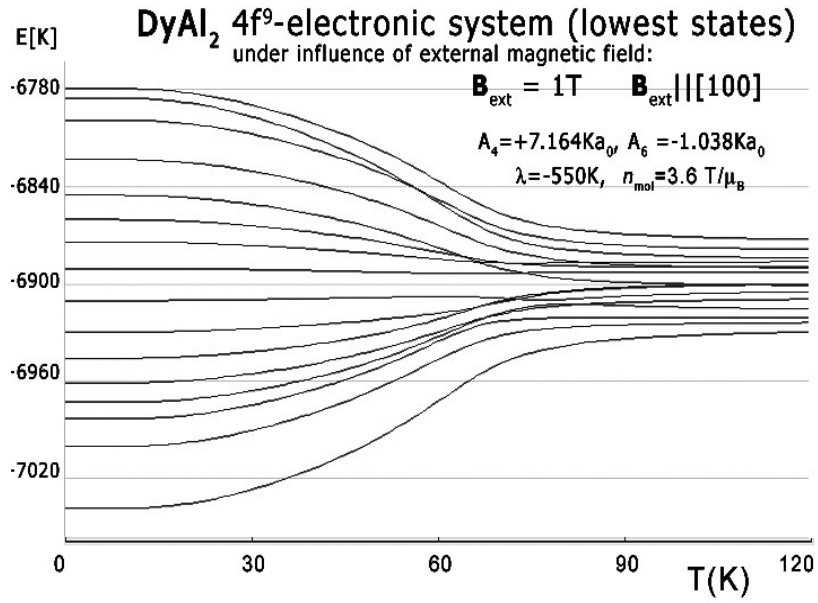

Fig. 5. Ground energy level structure vs. temperature calculated for $4f^9$ electronic system of Dy ions in $DyAl_2$ under the influence of external magnetic field $B_{ext} = 1$ T applied along the [100] direction. Parameters of CEF used in calculations and molecular field factor are shown.

Preprints (www.preprints.org) | NOT PEER-REVIEWED | Posted: 14 June 2018 doi:10.20944/preprints201806.0236.v1

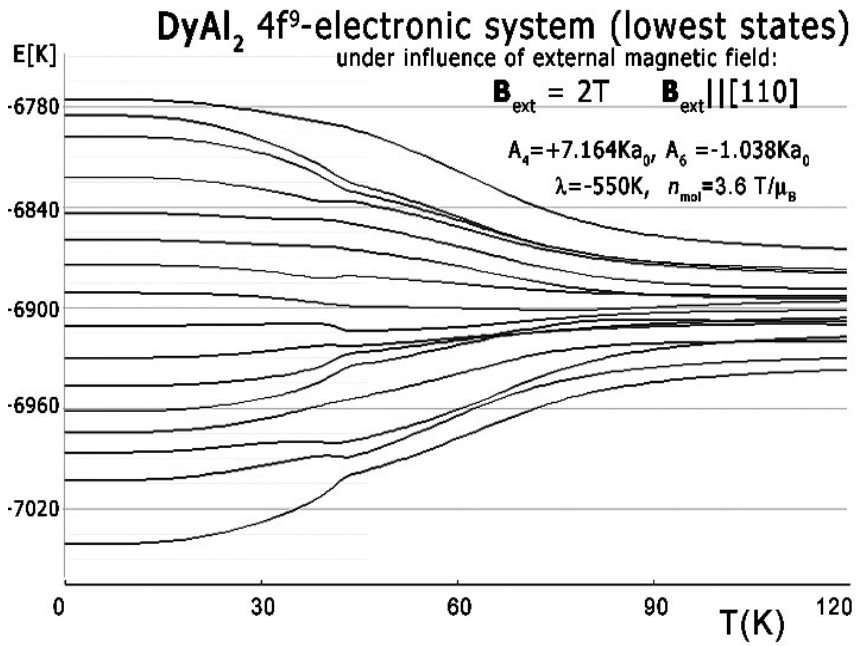

Fig. 6. Ground energy level structure vs. temperature calculated for $4f^9$ electronic system of Dy ions in $DyAl_2$ under the influence of external magnetic field B_{ext} = 2 T applied along the [110] direction. Parameters of CEF used in calculations and molecular field factor are shown.

Calculations of electronic structure under the influence of an external magnetic field applied along the [111] direction were also performed. Energy level structure calculated for external magnetic field in this direction does not contain anomalies and is similar to calculations performed for $\mathbf{B}_{ext}$ along the easy magnetization [100] direction, as shown in Fig. 5. Specific heat calculated in these conditions is shown in Fig. 8.

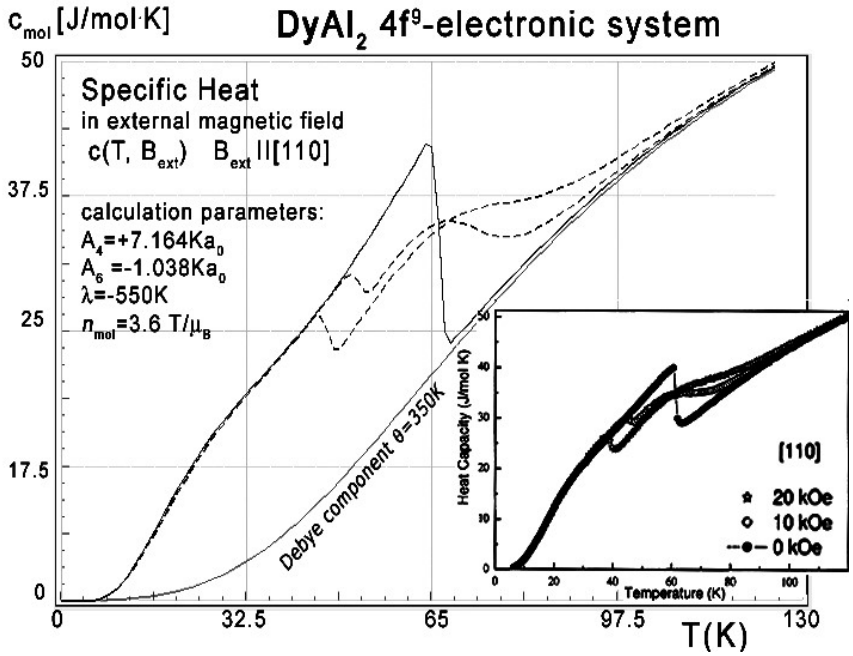

Fig. 7. Calculated 4*f*-electron component of molar specific heat (14) with Debye crystal lattice component (θ = 350K) vs. temperature for Dy ions in $DyAl_2$ under the influence of an external

Preprints (www.preprints.org) | NOT PEER-REVIEWED | Posted: 14 June 2018 doi:10.20944/preprints201806.0236.v1

magnetic field applied along the [110] direction. For comparison, the inset shows experimental data from [3] captured in the same external magnetic field conditions as simulated.

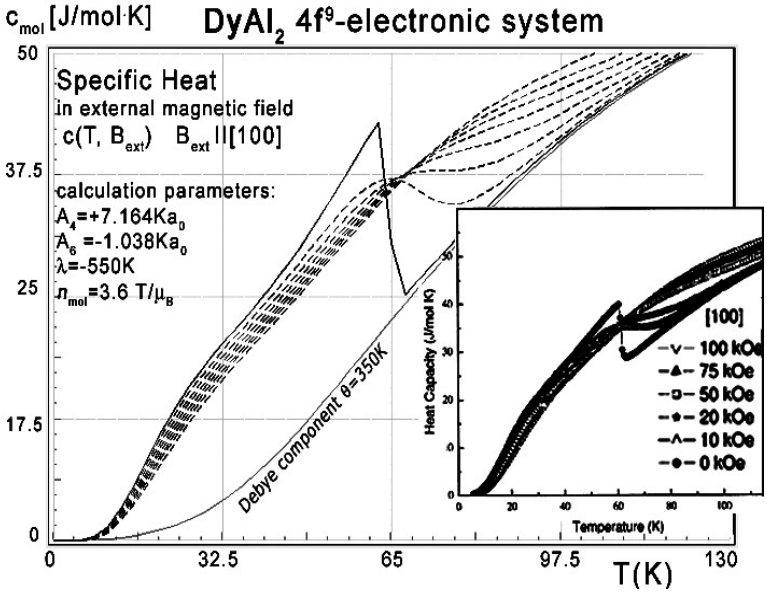

Fig. 8. Calculated 4*f*-electron component of molar specific heat (14) with Debye crystal lattice component ($\theta = 350$K) vs. temperature of Dy ions in $DyAl_2$ under the influence of an external magnetic field applied along the [100] direction. For comparison, the inset shows experimental data from [3] captured in the same external magnetic field conditions as simulated.

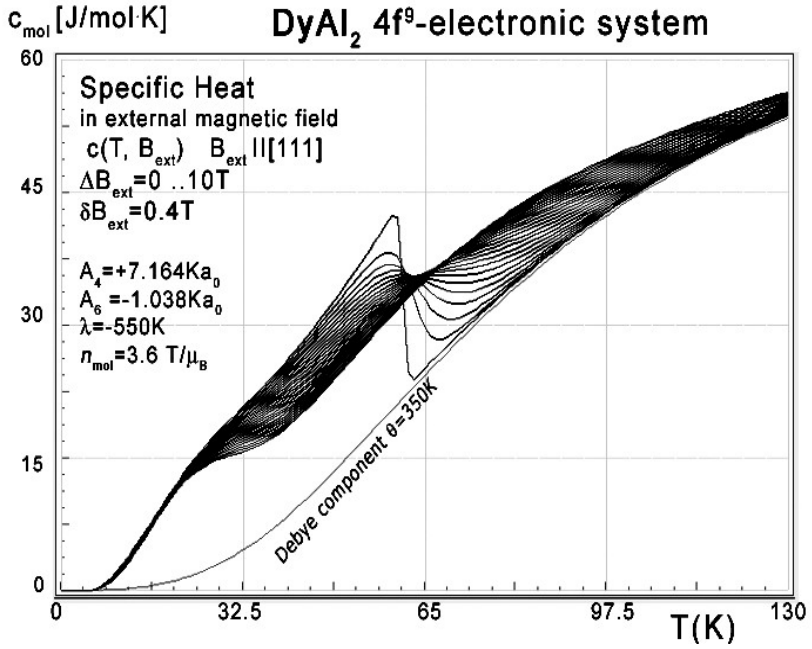

Fig. 9. Calculated 4*f*-electron component of molar specific heat (14) with Debye crystal lattice component ($\theta = 350$K) vs. temperature of Dy ions in $DyAl_2$ under the influence of an external magnetic field $\mathbf{B}_{ext}$ from 0 to 10 T applied along the [111] direction.

Collected data of specific heat makes it possible to calculate isothermal entropy change $-\Delta S(T,\mathbf{B}_{ext})$ according to (16), the same methodology as used by experimentalists [3-7]. Isothermal entropy

Preprints (www.preprints.org) | NOT PEER-REVIEWED | Posted: 14 June 2018 doi:10.20944/preprints201806.0236.v1

change calculated with various external magnetic fields applied along all main directions of cubic structure is presented in Figs. 10, 11 and 12. The reference data taken from experimental measurement [3] is shown in the insets.

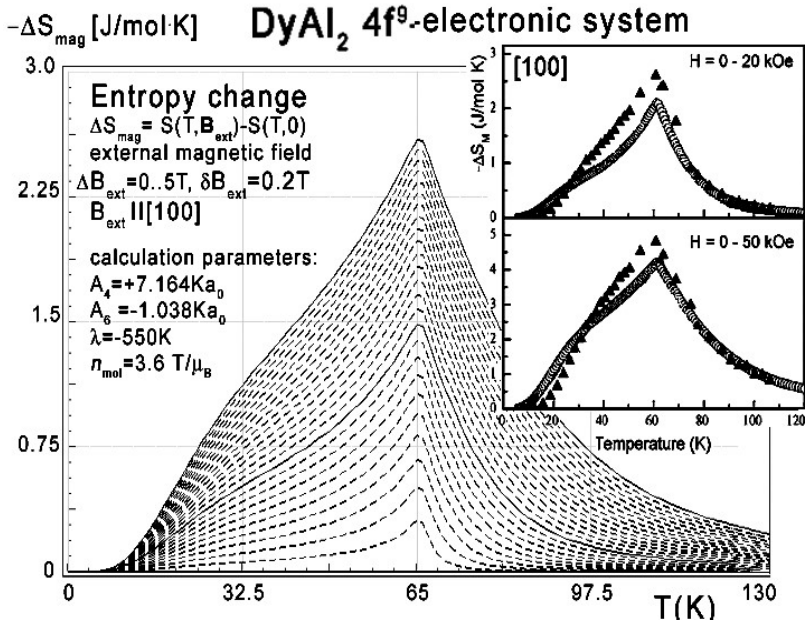

Fig. 10. Calculated isothermal entropy change of 4*f*-electronic system vs. temperature (16) of Dy ions in $DyAl_2$ under the influence of various values of external magnetic field from 0 to 5 T with step 0.2 T applied along the [100] direction. Inset: isothermal entropy change obtained from experimental data; black triangles - extracted from the magnetization, circles - extracted from specific heat, for the $DyAl_2$ single crystal aligned along the same direction, taken from [3]. The solid lines are congruent with the experimental data calculated for the B_{ext} = 2 T and B_{ext} = 5 T.

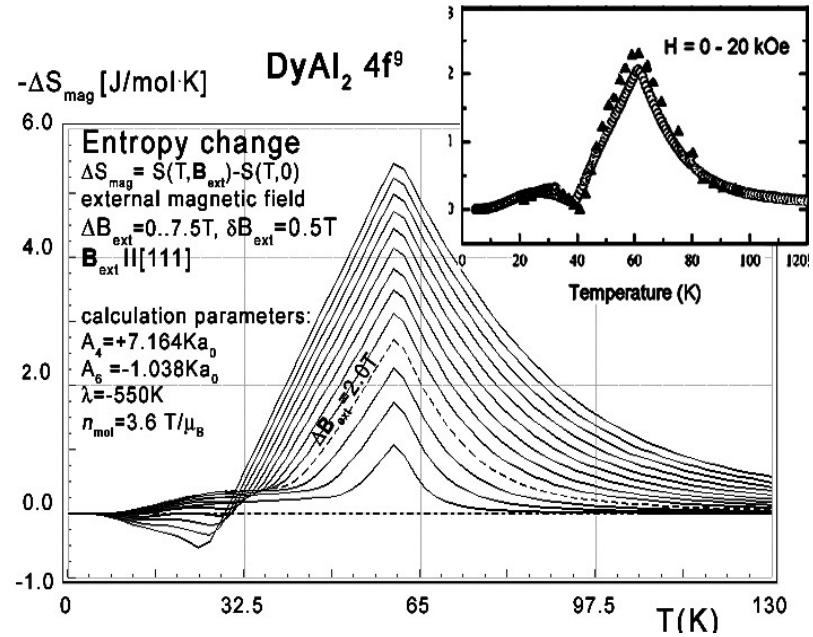

Fig. 11. Calculated isothermal entropy change vs. temperature (16) for various values of external magnetic fields from 0 to 2 T with step 0.1 T, applied along the [110] direction of $DyAl_2$ crystal lattice. Inset: black triangles show isothermal entropy change obtained from experimental data extracted from the magnetization; empty circles show specific heat for a $DyAl_2$ single crystal aligned along the same direction, taken from [3].

Preprints (www.preprints.org) | NOT PEER-REVIEWED | Posted: 14 June 2018 doi:10.20944/preprints201806.0236.v1

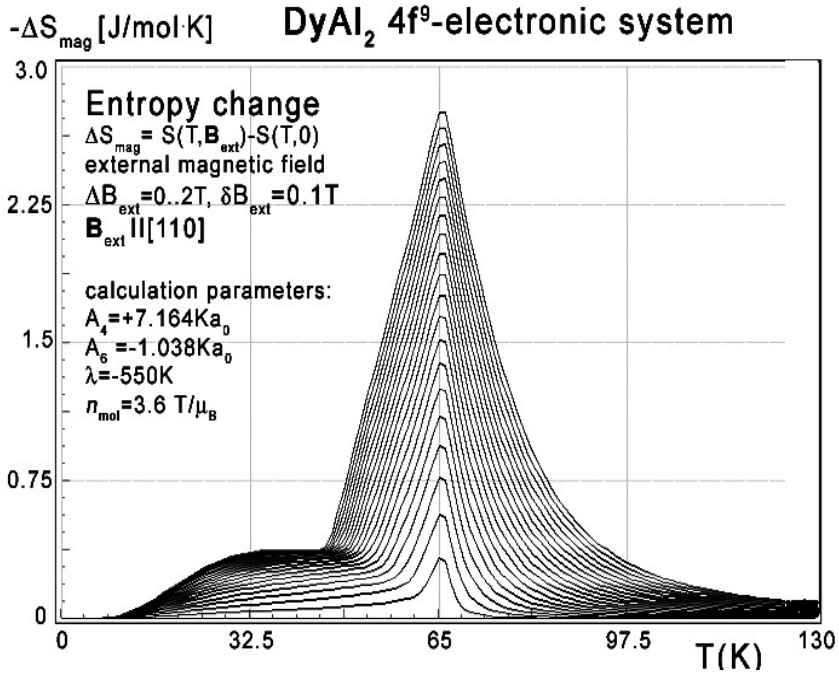

Fig. 12. Calculated isothermal entropy change of $DyAl_2$ vs. temperature (16) for various values of external magnetic field from 0 to 2 T with step 0.1 T applied along the diagonal [110] direction.

The anisotropic behavior of calculated thermomagnetic properties is reflected in the magnetocrystalline anisotropy constant calculations. The results of $K_i(T)$ calculations according to (17) in the absence of external magnetic field are shown in Fig. 13.

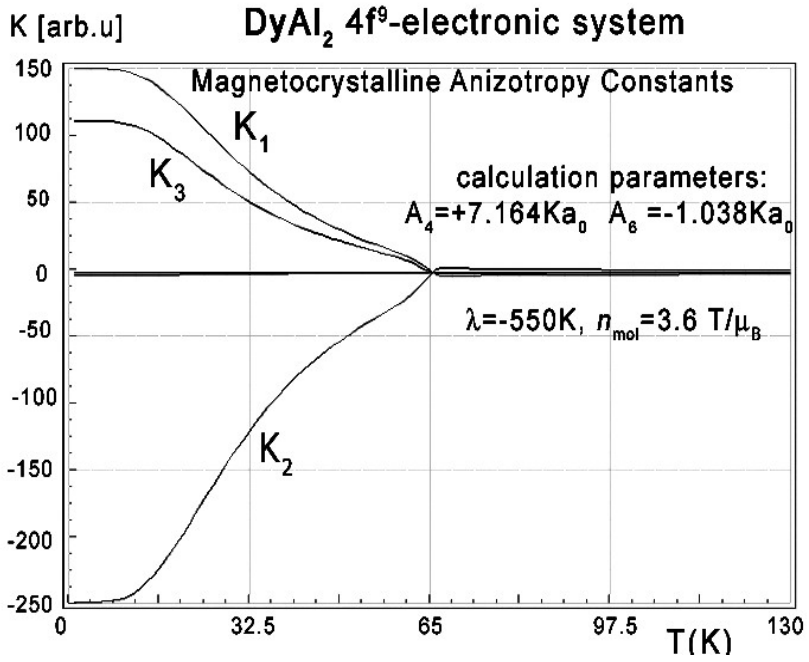

Fig. 13. Calculated according to (17), magnetocrystalline anisotropy constants K_1, K_2 and K_3 vs. temperature, calculated for Dy ions in $DyAl_2$ under the influence of CEF and molecular magnetic field.

For completeness, magnetic moment calculations vs. temperature under various external magnetic field conditions were performed. The results of $\mathbf{m}(T,\mathbf{B}_{ext})$ are presented in Figs. 14, 15 and 16. Fig. 14 clearly confirms the [100] direction as an easy magnetization axis. The applied external magnetic field

Preprints (www.preprints.org) | NOT PEER-REVIEWED | Posted: 14 June 2018 doi:10.20944/preprints201806.0236.v1

along this direction confirms perfect parallel directions of magnetic vector and external magnetic field (note: in cubic symmetry [100] = [010] = [001]).

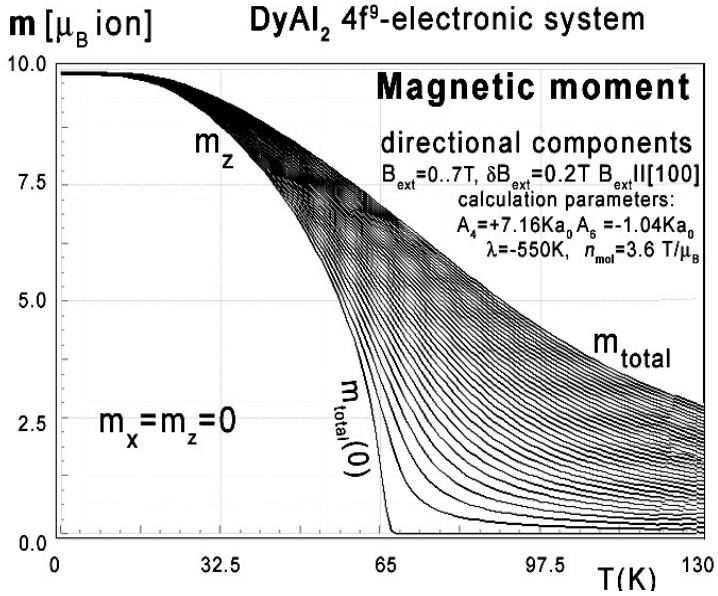

Fig. 14. Calculated x,y,z-directional components of total magnetic moment vs. temperature, calculated for Dy ions in $DyAl_2$ under the influence of CEF and molecular magnetic field and various values of external magnetic field from 0 to 7 T with step 0.2 T applied along the [100] direction.

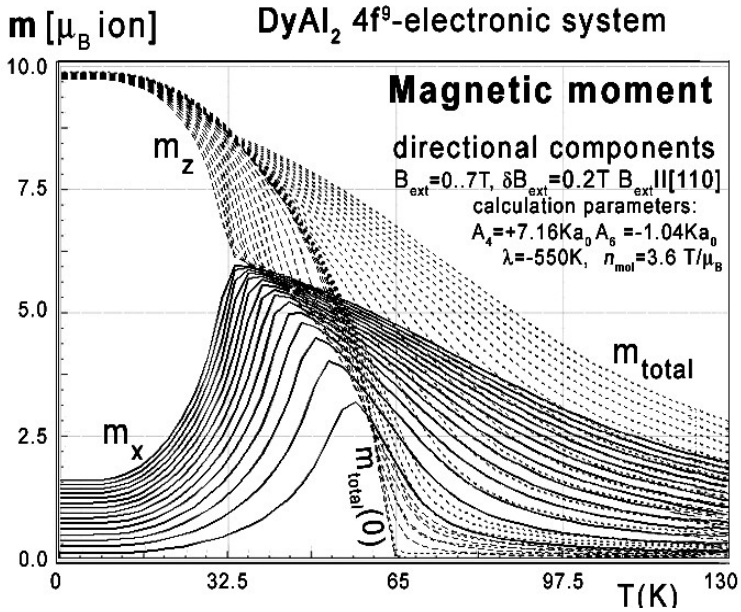

Fig. 15. Calculated x components (solid lines), z-components (dashed lines) of total magnetic moment m_{total} (dotted lines) vs. temperature calculated for Dy ions in $DyAl_2$ under the influence of CEF, molecular magnetic field, and various values of external magnetic field from 0 to 7 T with step 0.2 T applied along the [110] direction.

Preprints (www.preprints.org) | NOT PEER-REVIEWED | Posted: 14 June 2018 doi:10.20944/preprints201806.0236.v1

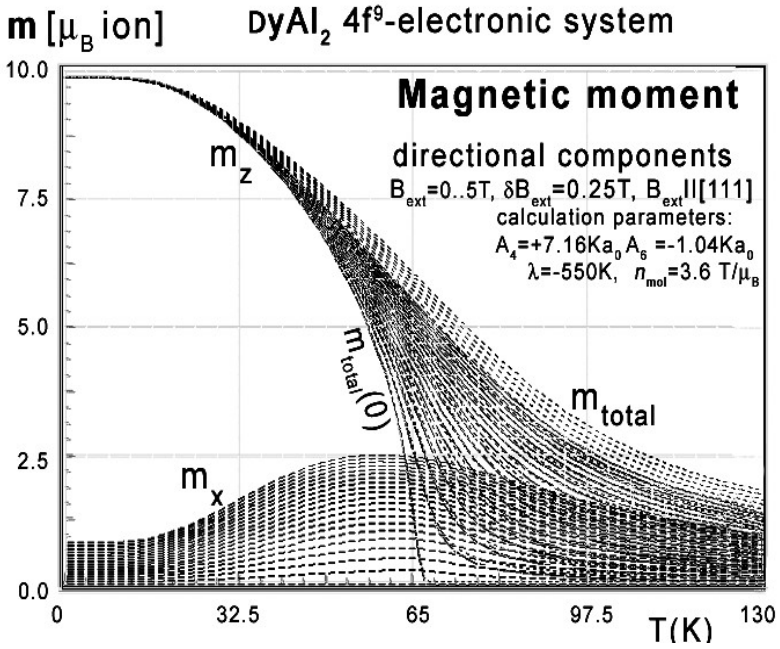

Fig. 16. Calculated x components (solid lines), z-components (dashed lines) of total magnetic moment m_{total} (dotted lines) vs. temperature, calculated for Dy ions in $DyAl_2$ under the influence of CEF, molecular magnetic field, and various values of external magnetic field from 0 to 7 T with step 0.2 T applied along the [111] direction.

Magnetic moment calculated in an external magnetic field parallel to the [110] direction reveals unusual behavior of the directional component of the total moment. Similar behavior of magnetic moment directions was reported in [3–5].

5. Calculation results for $HoAl_2$ and $ErAl_2$

Here we present the results of an investigation of the magnetic and magnetocaloric properties of a $HoAl_2$ and $ErAl_2$ single crystal. The predictions of properties are completely achieved without free parameters. We use established cubic CEF for $DyAl_2$ parameters in Stevens notation from [4] and recalculated them for Ho^{3+} and Er^{3+} ions.

As above, we attributed the magnetism of $HoAl_2$ and $ErAl_2$ and the magnetism of $HoAl_2$ to the Ho ions and performed calculations of the fine electronic structure of the $4f^{10}$ and $4f^{11}$ electronic systems, respectively. All calculations was performed for cubic symmetry, taking into account the crystal field and inter-site, spin-dependent exchange interactions. The energy level scheme derived is associated with the reduction of the degeneracy of the lowest atomic term (^{5}**I** and ^{4}**I** for Ho and Er ions, respectively) given by Hund's first two rules. The value of molecular field factor n_{mol} for $HoAl_2$ and $ErAl_2$ was established according to $n_{mol}^{Dy} = 3.6T/\mu_B$ for $DyAl_2$ and de Gennes scaling (18) [11]. The comparison between experimentally found Curie temperature T_C and de Gennes scaling is shown in Fig. 17.

Preprints (www.preprints.org) | NOT PEER-REVIEWED | Posted: 14 June 2018 doi:10.20944/preprints201806.0236.v1

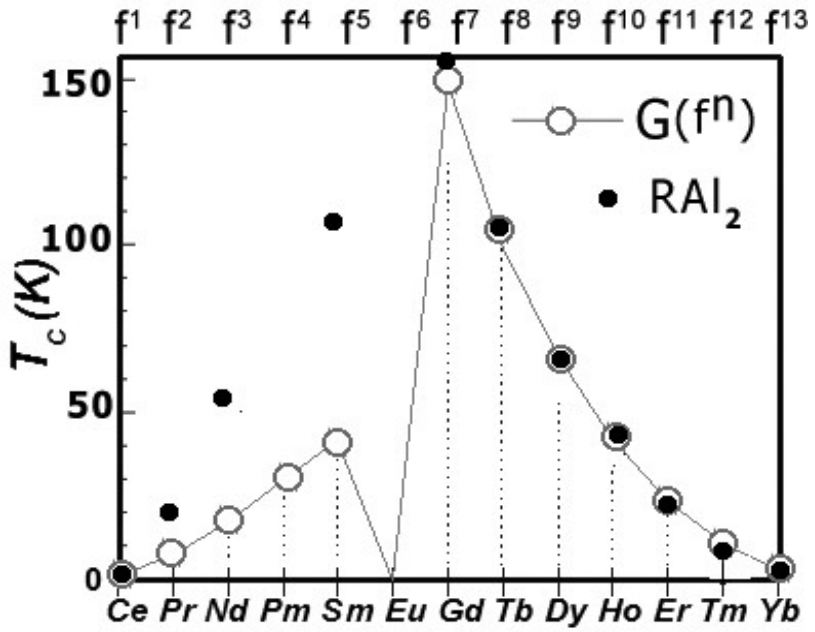

Fig. 17. De Gennes scaling of Curie temperature T_C for all rare-earth ions in series RAl_2 in comparison to experimental data from [4].

Experimental values of T_C for RAl_2 compounds [3-7] and the theory are in good agreement for heavy Rare Earths elements from Gd($4f^7$) to Yb($4f^{13}$). De Gennes relations [10, 14] make it possible to establish molecular field factor for $HoAl_2$ $n_{mol}^{Ho} = 2.1T/\mu_B$ and for $ErAl_2$ $n_{mol}^{Er} = 0.95T/\mu_B$.

5.1. Calculated properties of $HoAl_2$ single crystals

The electronic configuration of $_{67}Ho$ atoms consists of a closed shell inactive atomic core [$_{54}Xe$], electronic system $4f^{10}$ and outer electrons $5d^16s^2$. We attributed the magnetic properties of $HoAl_2$ compound as an effect of properties of $4f^{10}$ electronic system under the influence of electromagnetic interactions defined according to the description in the theory section. The starting point of our analysis is the ground atomic term ^5I with quantum number of orbital angular momentum L = 6 and total spin S = 2.

The full calculated energy level structure in $|L,S,L_z,S_z\rangle$ calculation space is shown in Fig. 18. The obtained overall splitting is strongly dependent on the strength of spin-orbit intra-atomic interactions. We used free-ion value of the spin-orbit constant of Ho^{3+} ions $\lambda = -780K$ [17] and obtained overall splitting of ^2F atomic term at about 20350K = 1.753 eV.

Details of ground states structure are shown in Fig. 18.

Preprints (www.preprints.org) | NOT PEER-REVIEWED | Posted: 14 June 2018 doi:10.20944/preprints201806.0236.v1

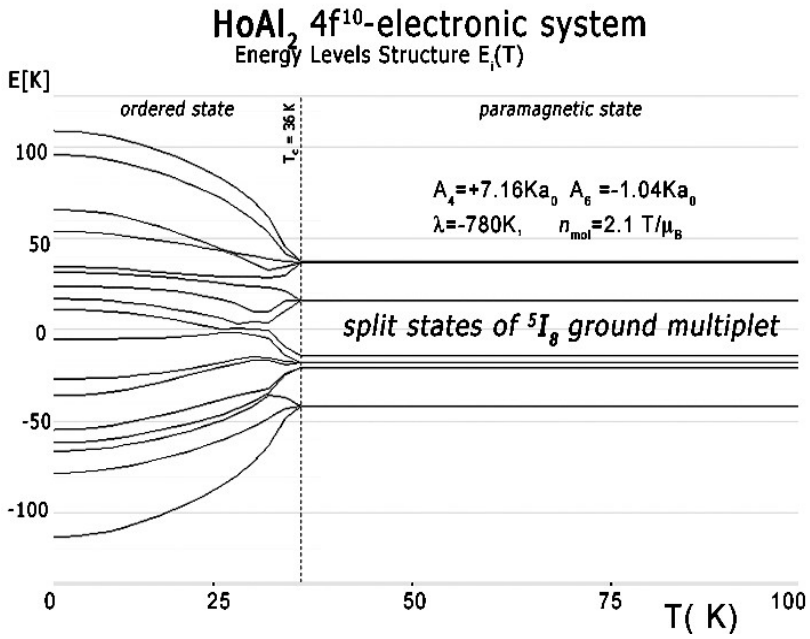

Fig. 18. The result of calculation of ground multiplet energy levels structure vs. temperature calculated of $4f^{10}$ electronic configuration of Ho ions in $HoAl_2$ in $|L,S,L_z,S_z\rangle$. At Curie temperature T_C = 36K the structure splits under the influence of a molecular field.

In the absence of an external magnetic field, the induced molecular field splits and moves into degenerated states. The value of the molecular field factor established for $HoAl_2$ which reproduces T_C well at about 36K is $n_{mol} = 2.1T/\mu_B$.

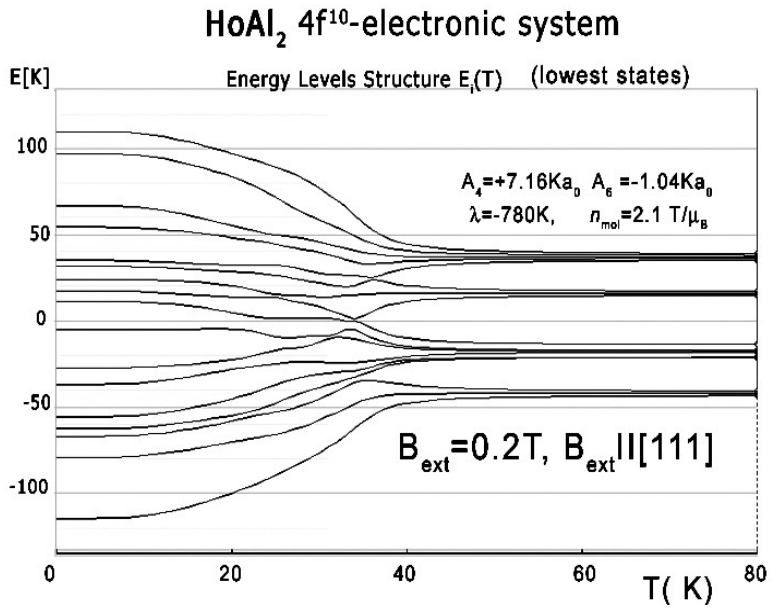

Fig. 19. Ground multiplet energy levels structure vs. temperature calculated for $4f^{10}$ electronic system of Ho ions in $HoAl_2$ under the influence of a small external magnetic field of 0.2 T applied along the [111] crystal direction.

Preprints (www.preprints.org) | NOT PEER-REVIEWED | Posted: 14 June 2018 doi:10.20944/preprints201806.0236.v1

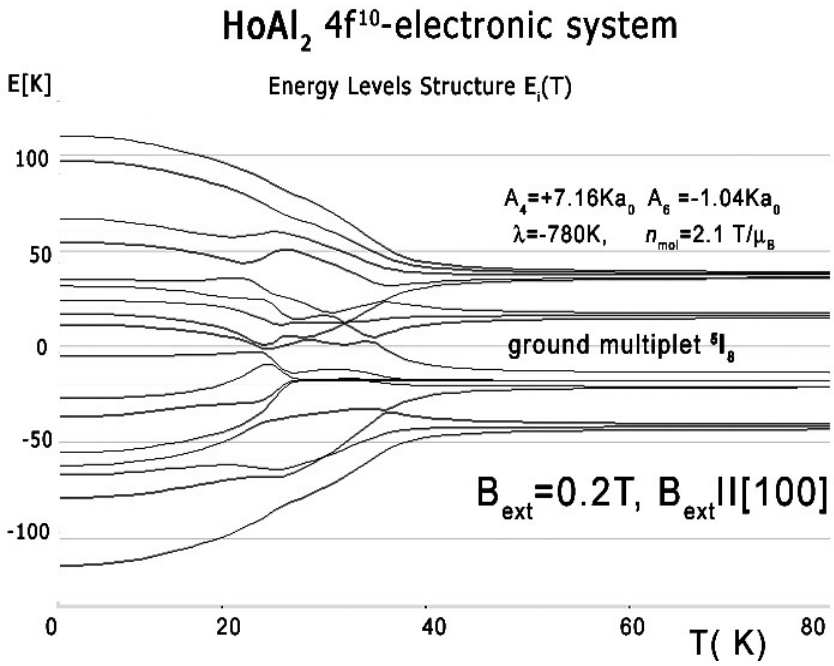

Fig. 20. Ground multiplet energy levels structure vs. temperature calculated for $4f^{10}$ electronic system of Ho ions in $HoAl_2$ under the influence of a small external magnetic field of 0.2 T applied along the [111] crystal direction.

Above T_C, in a paramagnetic state, the ground state is degenerated and consists of 3 states. The ground triplet wave functions of ground state of Ho ions ($4f^{10}$ electronic system) in $HoAl_2$ in a paramagnetic state can be expressed in $|Jz\rangle$ notation as:

$$\begin{aligned}\Gamma_1 &= +0.4|-6\rangle +0.583|-2\rangle -0.583|+2\rangle -0.4|+6\rangle \\ \Gamma_2 &= -0.086|-5\rangle-0.367|-1\rangle+0.5807|+3\rangle +0.72|+7\rangle \\ \Gamma_3 &= -0.086|+5\rangle-0.367|+1\rangle+0.581|-3\rangle +0.722|-7\rangle\end{aligned} \quad (24)$$

A molecular field splits these states at $T<T_C$. The value of the molecular field changes, and at T = 0 (absolute zero) B_{mol} = 13 T and its direction is along the [110] crystal direction. In this condition, the wave function of a ground singlet gets the form:

$$\begin{aligned}\Gamma_0 = &-0.291|-8\rangle+0.588|-7\rangle -0.410|-6\rangle +0.223|-5\rangle -0.257|-4\rangle +0.38|-3\rangle -0.312|-2\rangle +0.151|-1\rangle - \\ &0.014|0\rangle -0.081|+1\rangle +0.09|+2\rangle -0.040|+3\rangle +0.010|+4\rangle -0.011|+5\rangle +0.018|+6\rangle -0.012|+7\rangle \\ &+0.002|+8\rangle\end{aligned} \quad (25)$$

The electronic structure obtained in the absence of an external magnetic field is fragile; even a small magnetic field applied along the [100] or [111] direction forces the structure to change the order of states and creates an anomaly at low temperatures. The influence of a small external magnetic field applied along the [111] direction for the structure of the lowest electronic states is shown in Fig. 20. The position of this anomaly corresponds with peaks on specific heat curves. The calculated specific heat for a $HoAl_2$ single crystal under the influence of an external magnetic field applied along various crystal directions is presented in figures 21, 22 and 23.

Preprints (www.preprints.org) | NOT PEER-REVIEWED | Posted: 14 June 2018 doi:10.20944/preprints201806.0236.v1

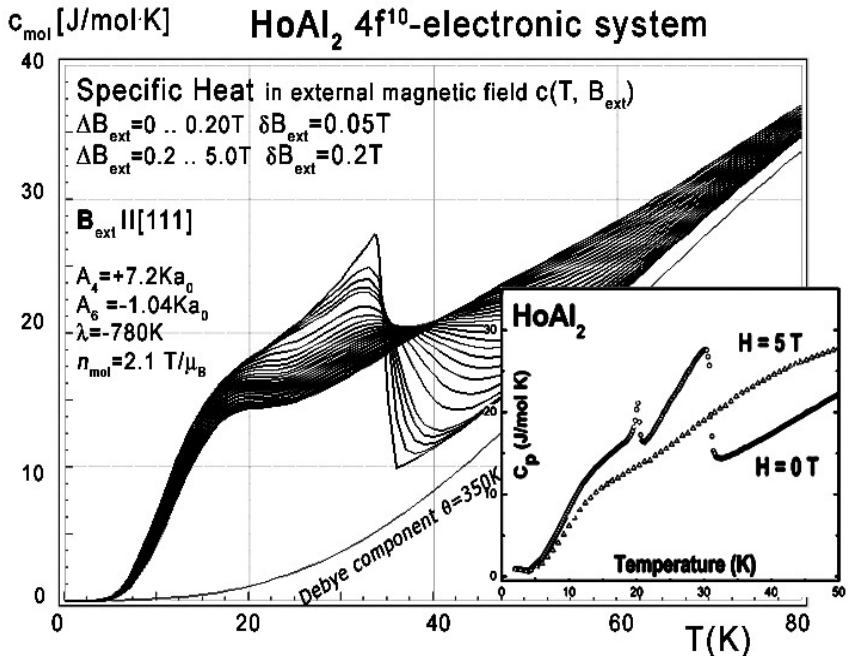

Fig. 21. Calculated $4f^{10}$-electronic system component of molar specific heat (14) with Debye crystal lattice component (θ = 350K) vs. temperature for Ho ions in $HoAl_2$ under the influence of an external magnetic field applied along the [100] direction. Inset: experimental data from [7].

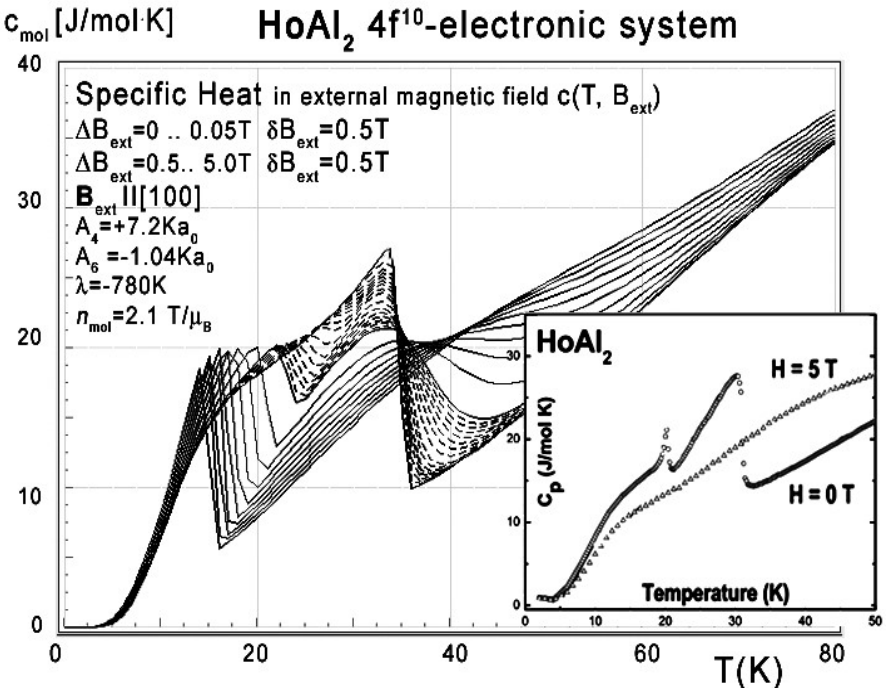

Fig. 22. Calculated molar specific heat (14) vs. temperature for Ho ions in $HoAl_2$ under the influence of an external magnetic field applied along the [100] direction. Inset: experimental data from [7].

Preprints (www.preprints.org) | NOT PEER-REVIEWED | Posted: 14 June 2018 doi:10.20944/preprints201806.0236.v1

The closer look at the unusual behaviour of the 4*f*-electron component of specific heat simulated under the influence of an external magnetic field along the diagonal [111] direction is shown in Fig. 23.

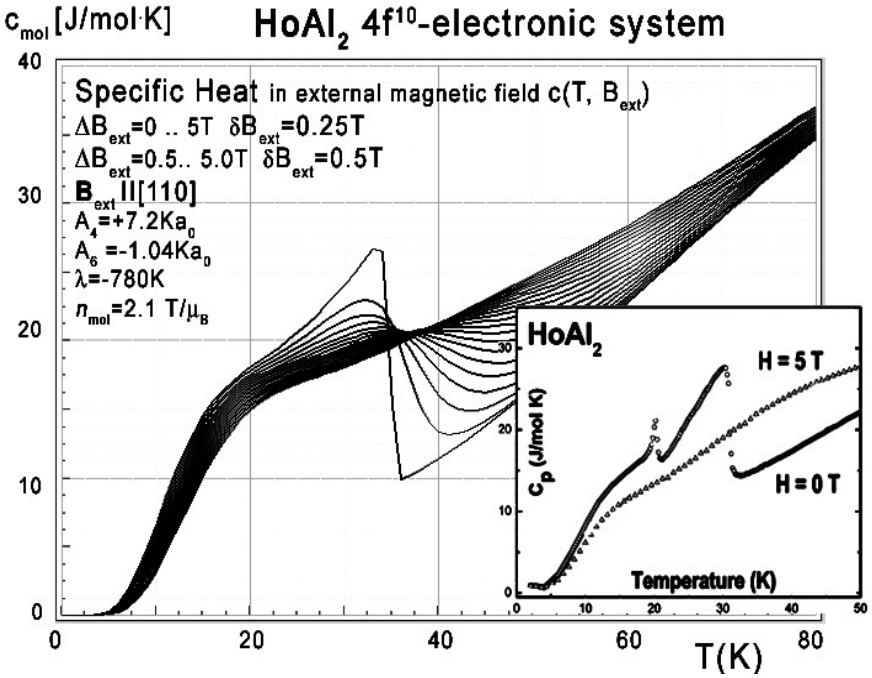

Fig. 23. Calculated molar specific heat (14) vs. temperature for Ho ions in $HoAl_2$ under the influence of an external magnetic field applied along easy magnetization axis in the [100] direction. Inset: experimental data from [7].

We have not found comparative experimental data for specific heat measurements, but F.W. Wang [19] provides data of measured specific heat change $\Delta c(T,B_{ext})$ defined as:

$$\Delta c(T,B_{ext}) = c(T,B_{ext}) - c(T,0) \quad (26)$$

for measurements for $\Delta B_{ext} = 5$ T. Comparison between data from [8] and our simulations of $\Delta c(T,B_{ext})$ is shown in Fig. 25. The simulation for $\Delta B_{ext} = 5$ T in this figure is represented by a solid line.

Collected data of specific heat makes it possible to calculate isothermal entropy change $-\Delta S(T,B_{ext})$ according to (16), the same methodology as used by experimentalist [3-7]. Isothermal entropy changes calculated with various external magnetic fields applied along all main directions of a cubic structure are presented in Figs. 24, 25 and 26.

Preprints (www.preprints.org) | NOT PEER-REVIEWED | Posted: 14 June 2018 doi:10.20944/preprints201806.0236.v1

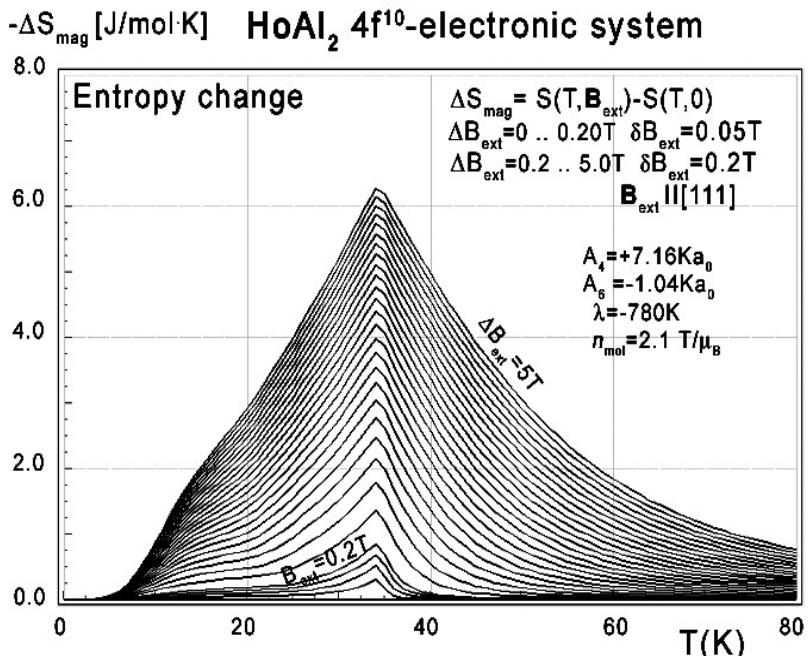

Fig. 24. Calculated isothermal entropy change of $4f^{10}$-electronic system vs. temperature (16) of Ho^{3+} ions in $HoAl_2$ under the influence of various external magnetic field values from 0 to 0.2 T with step 0.05 T and from 0 to 0.2 to 5.0 T with step 0.2 T applied along the [111] direction.

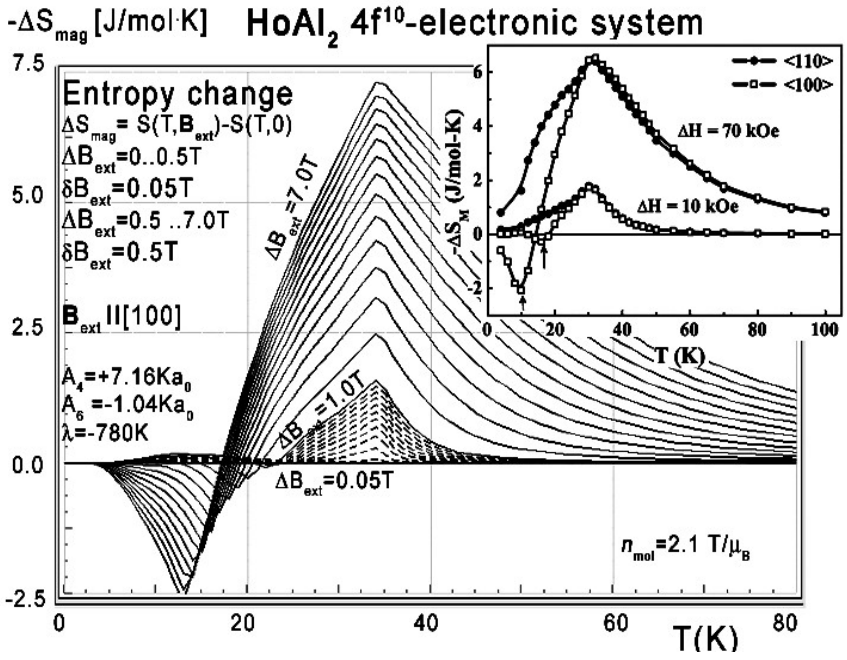

Fig. 25. Calculated isothermal entropy change of $4f^{10}$-electronic system vs. temperature (16) of Ho ions in $HoAl_2$ under the influence of various external magnetic field values from 0 to 0.5 T with step 0.05 T and from 0 to 0.5 to 7.0 T with step 0.5 T applied along the [100] direction. Inset: experimental data from [8].

Preprints (www.preprints.org) | NOT PEER-REVIEWED | Posted: 14 June 2018 doi:10.20944/preprints201806.0236.v1

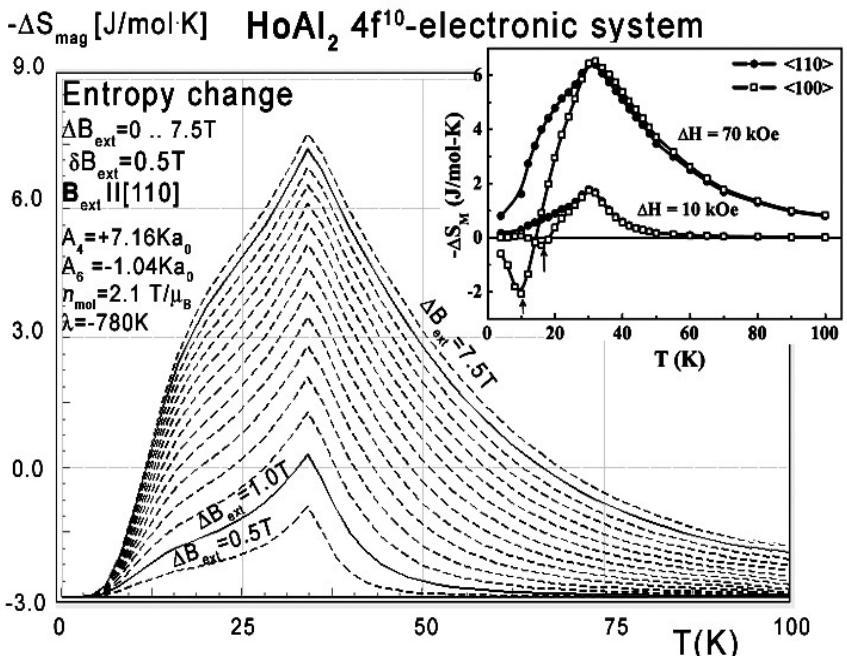

Fig. 26. Calculated isothermal entropy change of $4f^{10}$-electronic system vs. temperature (16) of Ho^{3+} ions in $HoAl_2$ under the influence of various external magnetic field values from 0 to 7.5 T with step 0.5 T applied along the [111] direction. Inset: experimental data from [8].

The anisotropic behavior of calculated thermomagnetic properties is reflected in magnetocrystalline anisotropy constant calculations. The results of $K_i(T)$ calculations according to (17) in the absence of an external magnetic field are shown in Fig. 27.

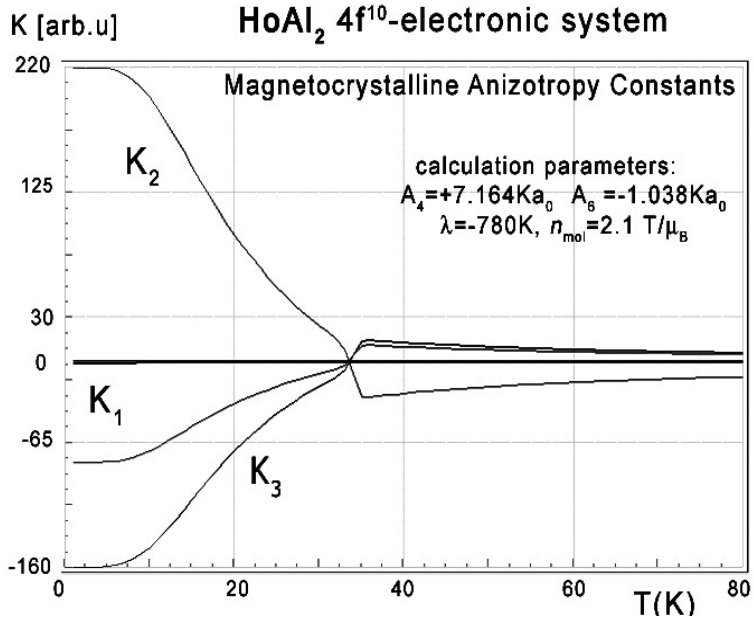

Fig. 27. Magnetocrystalline anisotropy constants K_1, K_2 and K_3 vs. temperature for Ho ions in $HoAl_2$ in absence of external magnetic field according to (17).

The results of $K_i(T)$ calculations according to (17) under the influence of external magnetic field $\mathbf{B}_{ext} = 1$ T applied along the [100] direction are shown in Fig. 28.

Preprints (www.preprints.org) | NOT PEER-REVIEWED | Posted: 14 June 2018 doi:10.20944/preprints201806.0236.v1

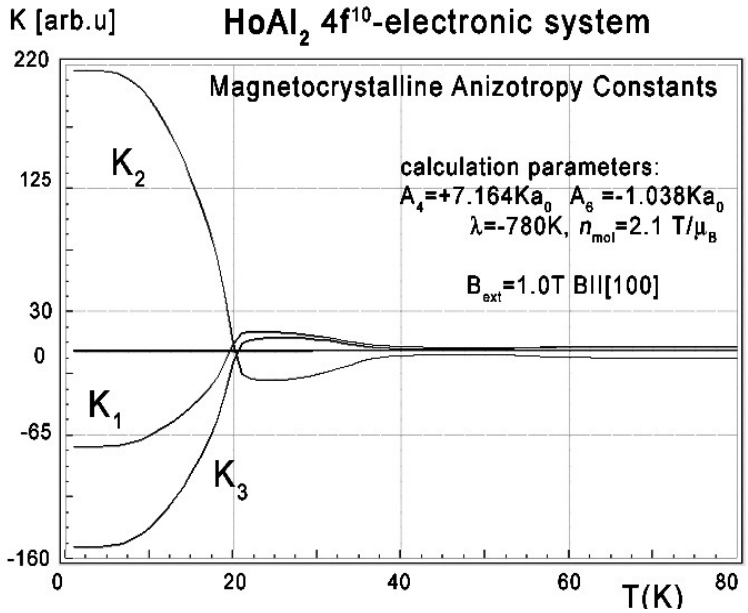

Fig. 28. Magnetocrystalline anisotropy constants K_1, K_2 and K_3 vs. temperature for Ho ions in $HoAl_2$ under the influence of CEF and molecular magnetic field calculated according to (17).

For completeness, magnetic moment calculations vs. temperature under various external magnetic field conditions were performed. The results of $\mathbf{m}(T,\mathbf{B}_{ext})$ are presented in Figs. 29, 30 and 31. The simulated thermal evolution of magnetic moment components under the influence of external magnetic field along the [110] direction shown in Fig. 30 clearly confirms the [110] direction as an easy magnetization axis of $HoAl_2$ in lowest temperatures. The applied external magnetic field along this direction confirms perfect parallel directions of magnetic vector and induced external magnetic field.

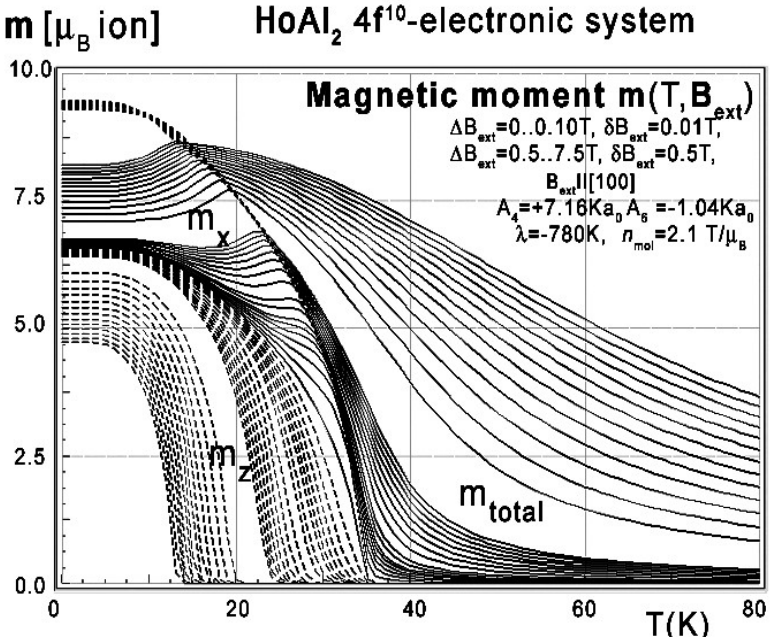

Fig. 29. Calculated x,y,z-directional components of total magnetic moment vs. temperature, calculated for Ho ions in $HoAl_2$ under the influence of various external magnetic field values from 0 to 0.1 T with step 0.01 T and from 0.5 to 7.5 T with step 0.5 T applied along the [100] direction.

Preprints (www.preprints.org) | NOT PEER-REVIEWED | Posted: 14 June 2018 doi:10.20944/preprints201806.0236.v1

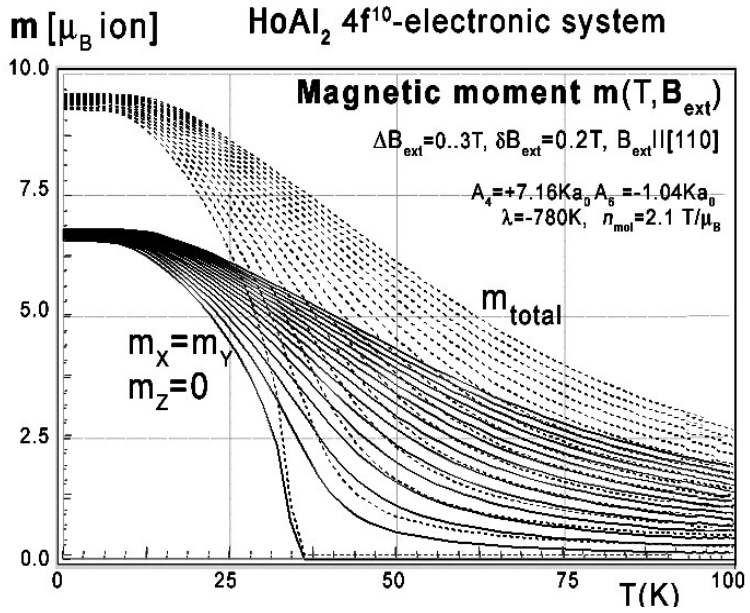

Fig. 30. Calculated x-components (solid lines), z-components (dashed lines) of total magnetic moment m_{total} (dotted lines) vs. temperature, calculated for Ho ions in $HoAl_2$ under the influence of CEF, molecular magnetic field and various values of external magnetic field from 0 to 3 T with step 0.2 T applied along the [110] direction.

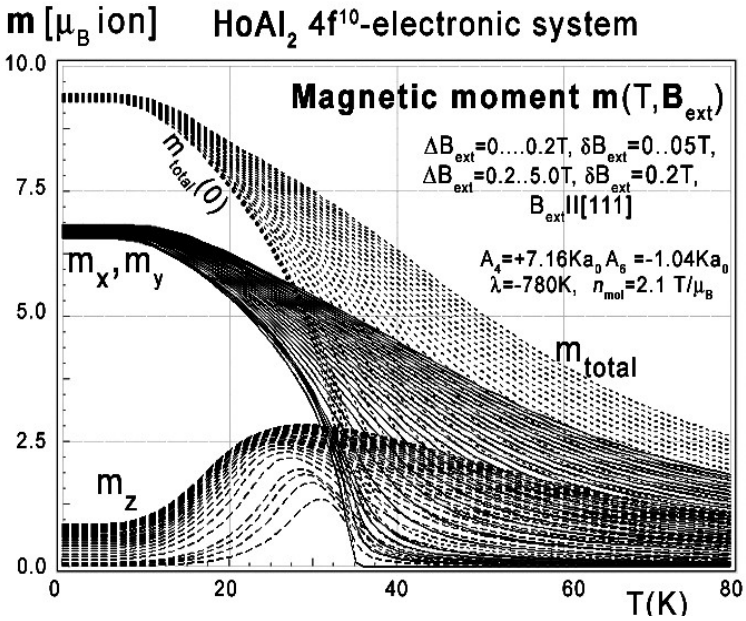

Fig. 31. Calculated x,y,z-directional components of total magnetic moment vs. temperature, calculated for Ho ions in $HoAl_2$ under the influence of CEF and molecular magnetic field and various values of external magnetic field from 0 to 0.2 T with step 0.05 T and from 0.2 to 5.0 T with step 0.2 T applied along the [111] direction.

Magnetic moment calculated in external magnetic field parallel to the [111] and [100] direction reveals unusual behavior of the directional component of total moment. Similar behavior of magnetic moment directions was reported in [20], but most of the presented results of calculations of properties of $HoAl_2$ still await experimental verification.

We found only a few reports about measurements of thermomagnetic properties of $HoAl_2$ single crystals. Some experimental comparative data of isothermal entropy change measured on $HoAl_2$

Preprints (www.preprints.org) | NOT PEER-REVIEWED | Posted: 14 June 2018 doi:10.20944/preprints201806.0236.v1

single crystals is provided by L.A. Gil et al. [7], and interesting entropy change is provided by M. Patra et al. [8]. All experimental data from [4, 5] confirms the correctness of our approach in thermomagnetic properties calculations of $HoAl_2$.

5.2. Calculation of properties of $ErAl_2$ single crystals

The electronic configuration of Er atoms consists of a closed shell inactive atomic core [$_{54}$Xe], electronic system $4f^{11}$ and 'outer electrons' $5d^16s^2$. We attribute the magnetic properties of $ErAl_2$ compound to be an effect of properties of $4f^{11}$ electronic system under the influence of electromagnetic interactions defined according to the description in the theory section. The starting point of our analysis is the ground atomic term ^{4}I with quantum number of orbital angular momentum L = 6 and total spin S = 3/2.

The full calculated energy level structure in $|L,S,L_z,S_z\rangle$ calculation space reveals good separation of ground multiplet $^4I_{15/2}$ states from the rest of eigenstates of the fine electronic structure. The overall energy levels splitting is strongly dependent on the strength of spin-orbit intra-atomic interactions. We used free-ion value of the spin-orbit constant of Er^{3+} ions λ = -1170K [17] and obtained overall splitting of ^{4}I atomic term at about 22900K = 1.97 eV. Details of ground multiplet $^4I_{15/2}$ states structure are shown in Fig. 32.

In the absence of an external magnetic field, the induced molecular field at $T < T_C$ splits degenerated states. The value of the molecular field factor established according to de Gennes scaling [16] for $ErAl_2$ which reproduces T_C well at about 11K is $n_{mol} = 0.95T/\mu_B$. Above T_C, in a paramagnetic state, the ground state is degenerated. The ground quartet consists of two quasi-doublets. The wave functions of ground state of Er ($4f^{11}$ electronic system) ions in $ErAl_2$ in a paramagnetic state can be expressed in $|Jz\rangle$ notation as:

$$\begin{aligned}\Gamma_1 &= -0.44|-6.5\rangle + 0.72|-2.5\rangle + 0.458|+1.5\rangle - 0.29|+5.5\rangle \\ \Gamma_1^* &= -0.44|+6.5\rangle + 0.72|+2.5\rangle + 0.458|-1.5\rangle - 0.28|-5.5\rangle \\ \Gamma_2 &= -0.61|-7.5\rangle + 0.78|-3.5\rangle + 0.143|+0.5\rangle - 0.04|+4.5\rangle \\ \Gamma_2^* &= 0.61|+7.5\rangle 0.781|+3.5\rangle + 0.14|-0.5\rangle + -0.04|-4.5\rangle\end{aligned} \quad (25)$$

A molecular field split these states at $T < T_C$. The value of the molecular field changes, and at T = 0 (absolute zero) B_{mol} = 4.46 T and its direction is along the [110] crystal direction. In this condition the wave function of a ground singlet gets the form:

$$\begin{aligned}\Gamma_0 = &-0.483|-7.5\rangle + 0.32|-6.5\rangle - 0.111|-5.5\rangle - 0.12|-4.5\rangle + + 0.577|-3.5\rangle - 0.459|-2.5\rangle + 0.159|-1.5\rangle - 0.029|-0.5\rangle \\ &+ 0.104|+0.5\rangle - 0.185|+1.5\rangle + 0.116|+2.5\rangle - 0.03|+3.5\rangle - -0.017|+4.5\rangle + 0.066|+5.5\rangle - 0.048|+6.5\rangle + 0.015|+7.5\rangle\end{aligned} \quad (26)$$

Preprints (www.preprints.org) | NOT PEER-REVIEWED | Posted: 14 June 2018 doi:10.20944/preprints201806.0236.v1

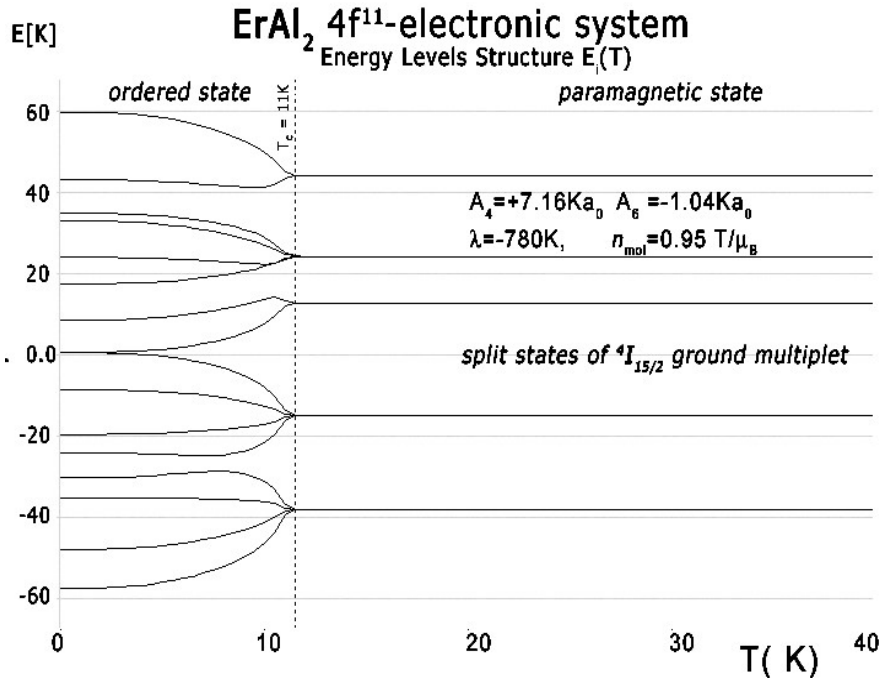

Fig. 32. The result of calculation of energy level positions vs. temperature of the fine electronic structure of $4f^{11}$ electronic configuration of Er ions in $ErAl_2$.

The structure of states is sensitive on external magnetic field influence. The effect of an external magnetic field B_{ext} = 1 T applied along the [111] direction for the structure of the lowest electronic states is shown in Fig. 33.

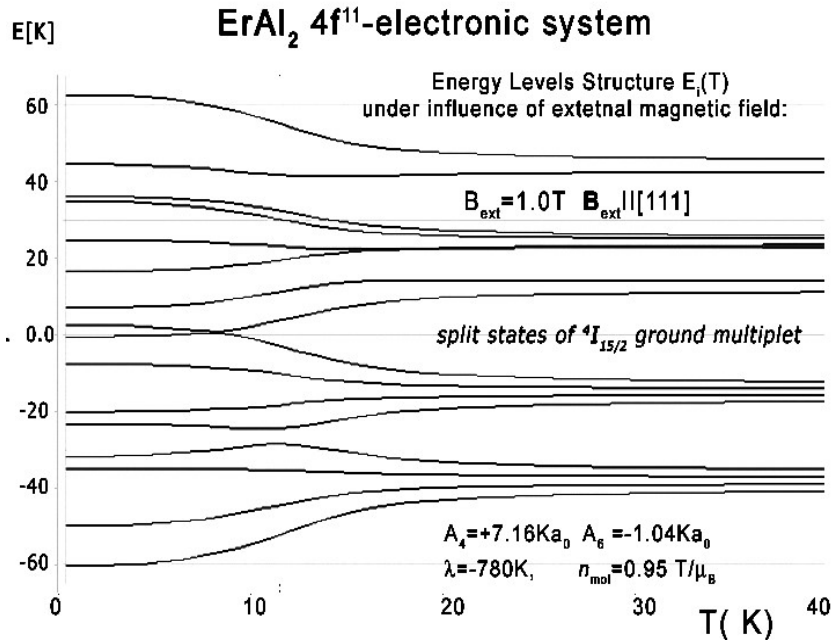

Fig. 33. Calculated energy level structure of $4f^{11}$ electronic system of Er ions vs. temperature under the influence of external magnetic field B_{ext} = 1 T applied along the [111] direction.

Preprints (www.preprints.org) | NOT PEER-REVIEWED | Posted: 14 June 2018 doi:10.20944/preprints201806.0236.v1

The energy level structure makes it possible to calculate the 4*f*-electron component of specific heat. The result of calculation of specific heat under the influence of an external magnetic field compared to experimental data from [21] is shown in Figs. 34, 35 and 36.

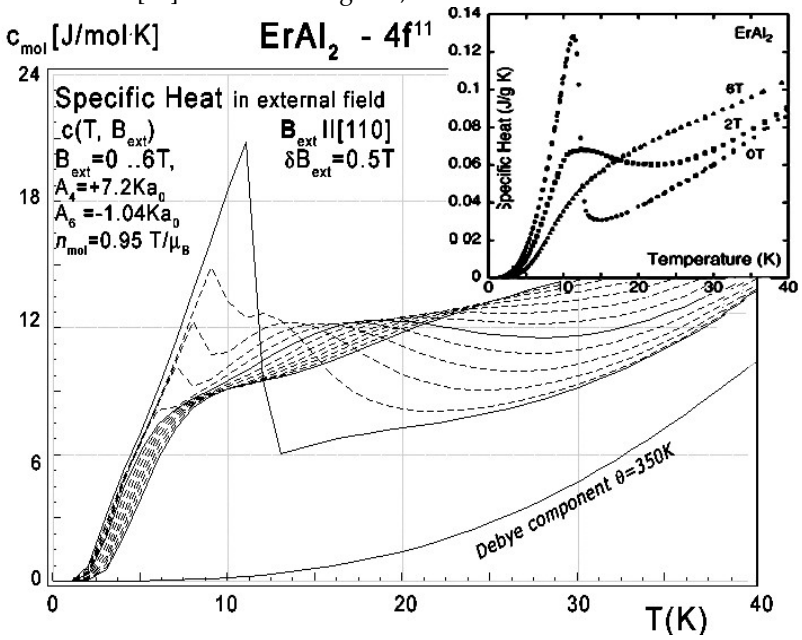

Fig. 34. Calculated $4f^{11}$-electronic system component of molar specific heat (14) with Debye crystal lattice component (θ = 350K) vs. temperature of Er ions in $ErAl_2$ under the influence of external magnetic field from 0 to 6 T with step 0.2 T. Inset: experimental data from [21] congruent with results calculated for $B_{ext} = 0$, $B_{ext} = 2.0$ T and $B_{ext} = 6.0$ T lines are solid lines.

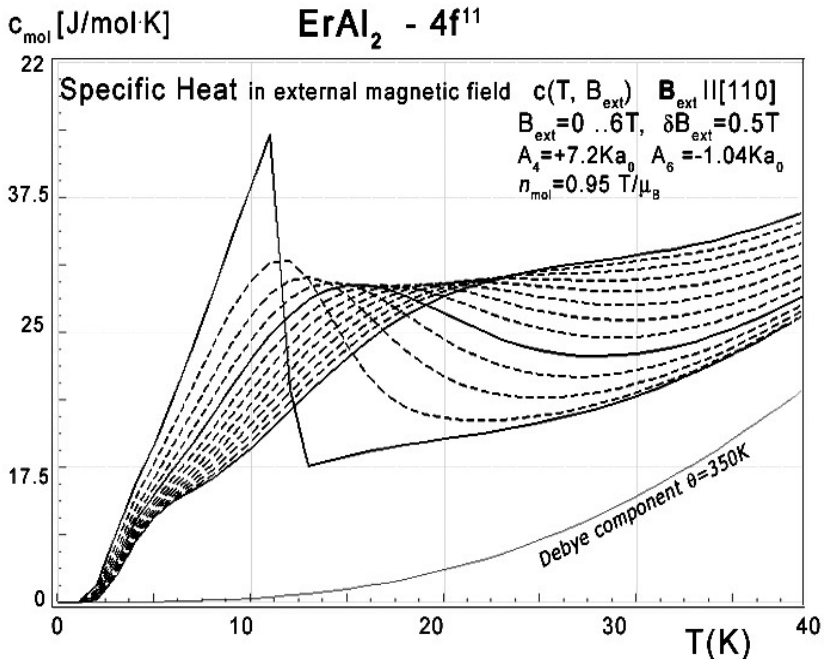

Fig. 35. Calculated $4f^{11}$-electronic system component of molar specific heat (14) with Debye crystal lattice component (θ = 350K) vs. temperature of Er ions in $ErAl_2$ under the influence of external magnetic field from 0 to 6 T with step 0.2 T.

Preprints (www.preprints.org) | NOT PEER-REVIEWED | Posted: 14 June 2018 doi:10.20944/preprints201806.0236.v1

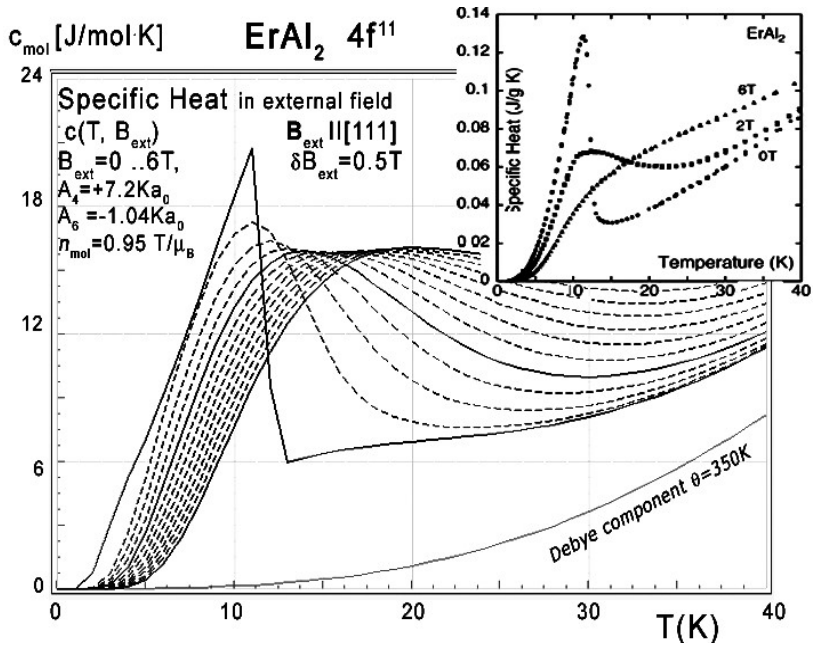

Fig. 36. Calculated $4f^{11}$-electronic system component of molar specific heat (14) with Debye crystal lattice component (θ = 350K) vs. temperature of Er ions in $ErAl_2$ under the influence of external magnetic field from 0 to 6 T with step 0.2 T. Inset: experimental data from [21] congruent with results calculated for B_{ext} = 0, B_{ext} = 2.0 T and B_{ext} = 6.0 T lines are solid lines.

Collected specific heat data makes it possible to calculate isothermal entropy change $-\Delta S(T,B_{ext})$ according to (16), the same methodology as used by experimentalist [3-8]. Isothermal entropy change calculated with various external magnetic fields is presented in Figs. 37, 38 and 39.

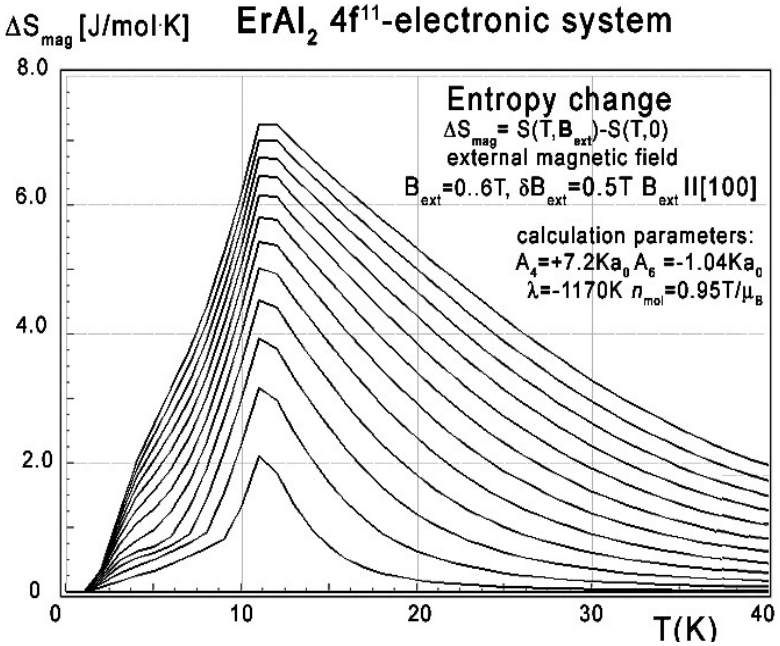

Fig. 37. Calculated isothermal entropy change of $4f^{11}$-electronic system vs. temperature (16) of Er ions in $ErAl_2$ under the influence of various values of external magnetic field from 0 to 6 T with step 0.2 T applied along the [100] direction.

Preprints (www.preprints.org) | NOT PEER-REVIEWED | Posted: 14 June 2018 doi:10.20944/preprints201806.0236.v1

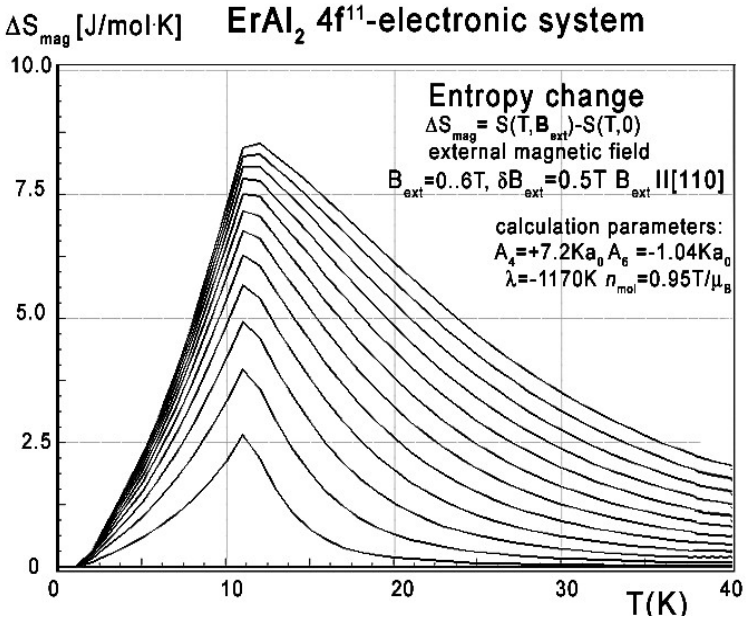

Fig. 38. Calculated isothermal entropy change vs. temperature (16) for various values of external magnetic field from 0 to 6.0 T with step 0.5 T, applied along the [110] direction of $ErAl_2$ crystal lattice.

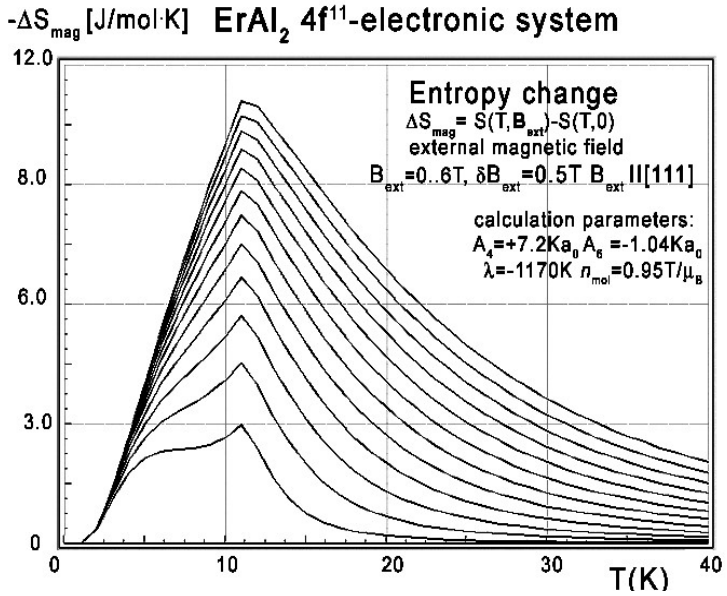

Fig. 39. Calculated isothermal entropy change of $ErAl_2$ vs. temperature (16) for various values of external magnetic field from 0 to 6 T with step 0.5 T applied along the diagonal [111] direction.

The anisotropic behavior of calculated thermomagnetic properties reflects in magnetocrystalline anisotropy constant calculations. The results of $K_i(T)$ calculations according to (17) in absence of external magnetic field are shown in Fig. 40.

Preprints (www.preprints.org) | NOT PEER-REVIEWED | Posted: 14 June 2018 doi:10.20944/preprints201806.0236.v1

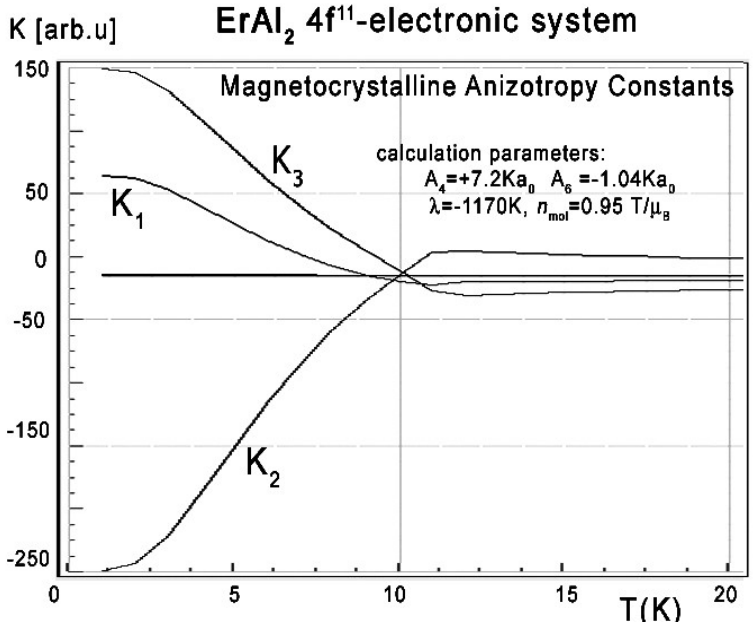

Fig. 40. Calculated magnetocrystalline anisotropy constants K_1, K_2 and K_3 vs. temperature (17), calculated for Er ions under the influence of CEF established for RAl_2 series and molecular magnetic field.

For completeness, magnetic moment calculations vs. temperature under various external magnetic field conditions was performed. The results of $\mathbf{m}(T,\mathbf{B}_{ext})$ are presented in Figs. 41, 42 and 43.

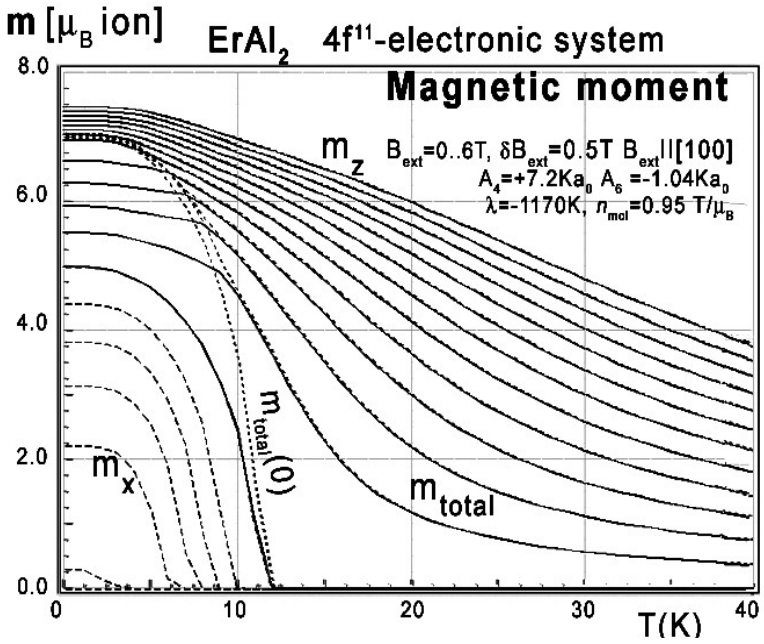

Fig. 41. Calculated x,y,z-directional components of total magnetic moment vs. temperature, calculated for Er ions in $ErAl_2$ under the influence of CEF and molecular magnetic field and various values of external magnetic field from 0 to 6 T with step 0.5 T applied along the [100] direction.

Preprints (www.preprints.org) | NOT PEER-REVIEWED | Posted: 14 June 2018 doi:10.20944/preprints201806.0236.v1

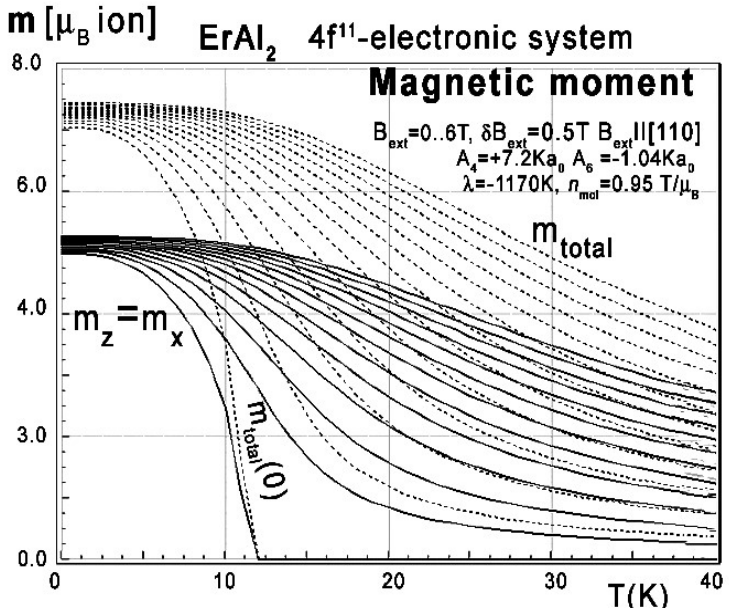

Fig. 42. Calculated x,y,z-directional components of total magnetic moment m_{total} (dotted lines) vs. temperature, calculated for Er ions in $ErAl_2$ under the influence of CEF, molecular magnetic field and various values of external magnetic field from 0 to 6 T with step 0.5 T applied along the [110] direction. $m_y(T) = 0$, x and z components of a magnetic moment are equally distributed.

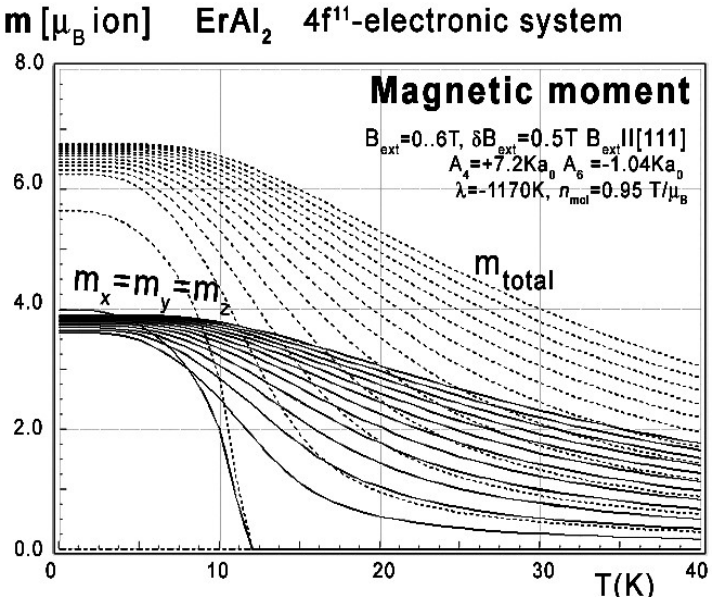

Fig. 43. Calculated x,y,z-directional components of the total magnetic moment m_{total} (dotted lines) vs. temperature, calculated for Er ions in $ErAl_2$ under the influence of CEF, molecular magnetic field and various values of external magnetic field from 0 to 6 T with step 0.5 T applied along the [111] direction. All directional magnetic moment components are equally distributed.

Magnetic moment calculated in external magnetic field parallel to [111] and [110] directions reveals unusual behavior of the directional component of total moment. The electronic system seems to be easy switchable between those crystallographic directions. The low-temperature easy magnetization axis along the [110] direction easy transforms into [111]. The external magnetic field under $B_{ext} < 0.01$ T changes directional components distribution of total magnetic moment of Er ions (compare Fig. 42 and Fig. 43).

Preprints (www.preprints.org) | NOT PEER-REVIEWED | Posted: 14 June 2018 doi:10.20944/preprints201806.0236.v1

Similar behavior of magnetic moment directions was reported in [7], but most of the presented results of calculations of properties of $ErAl_2$ still await experimental verification.

6. Calculated properties of $TbAl_2$, $SmAl_2$ and $GdAl_2$ single crystals

We performed electronic structure calculations for Tb^{3+}, Sm^{3+} and Gd^{3+} in the RAl_2 C-15 crystal structure. Details of obtained results was published in [22]. In this section we present selected results of thermomagnetic properties of these compounds.

6.1 Calculated thermomagnetic properties of $TbAl_2$

The $_{65}Tb$ atoms contain electronic structure that consists of a closed shell inactive atomic core $[_{54}Xe]$, electronic system $4f^8$ and outer electrons $5d^16s^2$. We attributed the magnetic properties of $TbAl_2$ compound as an effect of properties of $4f^8$ electronic system under the influence of electromagnetic interactions defined according to the description in the theory section. The starting point of our analysis is the ground atomic term ^2F with the quantum number of orbital angular momentum L = 3 and total spin S = 3.

The full calculated energy level structure in |L,S,Lz,Sz> calculation space is shown in Fig. 44. The obtained overall splitting is strongly dependent on the strength of spin–orbit intra-atomic interactions. We used free-ion value of spin-orbit constant of Tb^{3+} ions ◎ = -410K [13] and obtained overall splitting of ^2F atomic term at about 8620K = 0.743 eV.

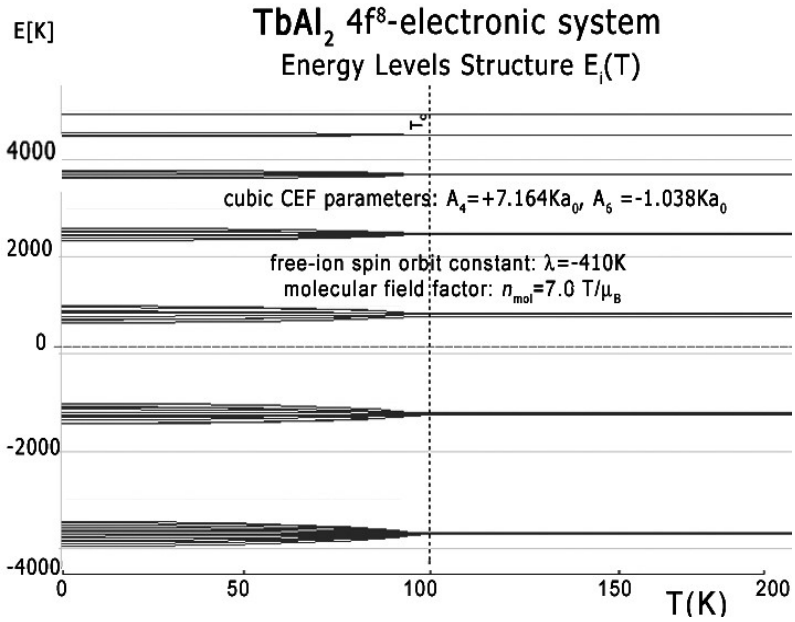

Fig. 44. The result of calculation of energy level positions vs. temperature of the fine electronic structure of $4f^8$ electronic configuration of Tb ions in $TbAl_2$ in |L,S,Lz,Sz> space under the influence of intra-atomic spin-orbit coupling, inter-atomic self-consistent molecular magnetic field and Crystal Electric Field (CEF).

In the absence of an external magnetic field, the induced molecular field splits degenerated states. The value of the molecular field factor established for $TbAl_2$ which reproduces T_C well at about 105K is $n_{mol} = 7.0T/\mu_B$.

Above T_C, in a paramagnetic state, the ground state is degenerated. The ground quartet consists of two quasi doublets. The wave functions of the ground state of Tb ($4f^8$ electronic system) ions in $TbAl_2$ in a paramagnetic state can be expressed in |Jz> notation as:

$$\Gamma_1 = +0.661|-4\rangle -0.353|0\rangle +0.6614|+4\rangle \quad (26)$$

Preprints (www.preprints.org) | NOT PEER-REVIEWED | Posted: 14 June 2018 doi:10.20944/preprints201806.0236.v1

$$\Gamma_2 = -0.151|-6\rangle - 0.691|-2\rangle + 0.691|+2\rangle + 0.151|+6\rangle$$
$$\Gamma_3 = -0.450|-3\rangle + 0.381|+1\rangle + 0.807|+5\rangle$$
$$\Gamma_4 = -0.450|+3\rangle + 0.381|-1\rangle + 0.808|-5\rangle$$

The molecular field splits these states at $T < T_C$. The value of the molecular field changes, and at $T = 0$ (absolute zero) $B_{mol} = 42$ T and its direction is along the crystal [110] direction. In this condition the wave function of a ground singlet gets the form:

$$\Gamma_0 = -0.358|-6\rangle + 0.567|-5\rangle - 0.553|-4\rangle + 0.407|-3\rangle - 0.247|-2\rangle + 0.122|-1\rangle - 0.04|0\rangle + 0.003|+1\rangle + 0.006|+2\rangle - 0.004|+3\rangle + 0.001|+4\rangle - 0.0002|+5\rangle + 0.0001|+6\rangle \quad (27)$$

The electronic structure obtained in the absence of an external magnetic field is extremely fragile; even a small magnetic field applied along [100] or [111] direction forces the structure to change the order of states and creates an anomaly at low temperatures. The influence of a small external magnetic field applied along [111] direction for the structure of the lowest electronic states is shown in Fig. 5(b). The position of this anomaly corresponds with peaks on specific heat curves. The calculated specific heat for a $TbAl_2$ single crystal under the influence of an external magnetic field applied along various crystal directions is presented in Fig. 45.

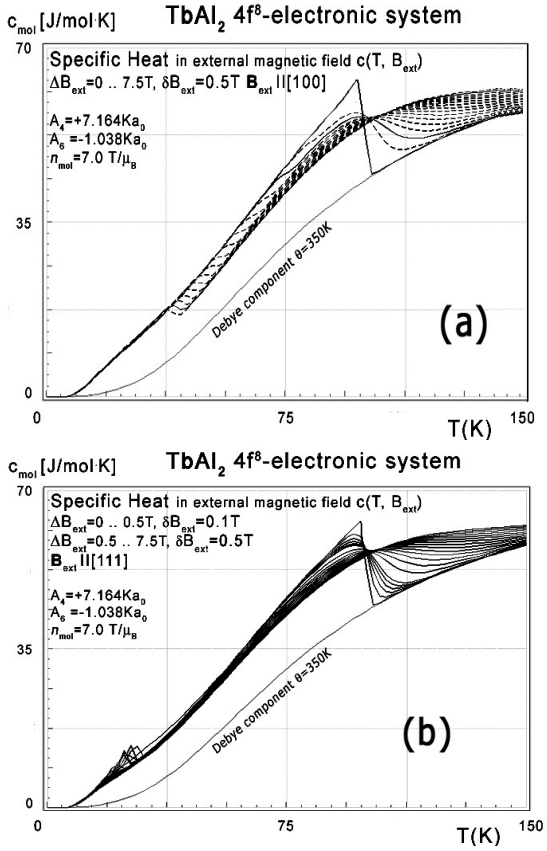

Preprints (www.preprints.org) | NOT PEER-REVIEWED | Posted: 14 June 2018 doi:10.20944/preprints201806.0236.v1

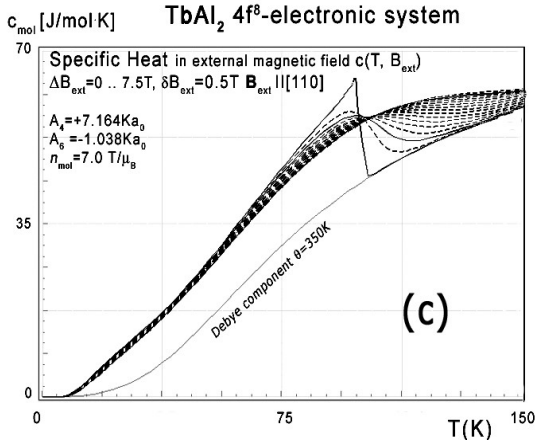

Fig. 45. Calculated 4*f*-electron component of molar specific heat (14) with Debye crystal lattice component (θ = 350K) vs. temperature for Tb ions in $TbAl_2$ **(a)** under the influence of an external magnetic field applied along [100] direction; **(b)** under the influence of an external magnetic field applied along [111] direction; **(c)** under the influence of an external magnetic field applied along [100] direction.

The closer look at the unusual behaviour of the 4*f*-electron component of specific heat simulated under the influence of an external magnetic field along 'diagonal' [111] direction is shown in Fig. 46(a).

We have not found comparative experimental data for specific heat measurements, but F.W. Wang [19] provides data of measured specific heat change $\Delta c(T,B_{ext})$ defined as:

$$\Delta c(T,B_{ext}) = c(T,B_{ext}) - c(T,0) \quad (29)$$

for measurements for $\Delta B_{ext} = 5$ T. Comparison between data from [5] and our simulations of $\Delta c(T,B_{ext})$ is shown in Fig. 46(b) The simulation for $\Delta B_{ext} = 5$ T in this figure is represented by a solid line.

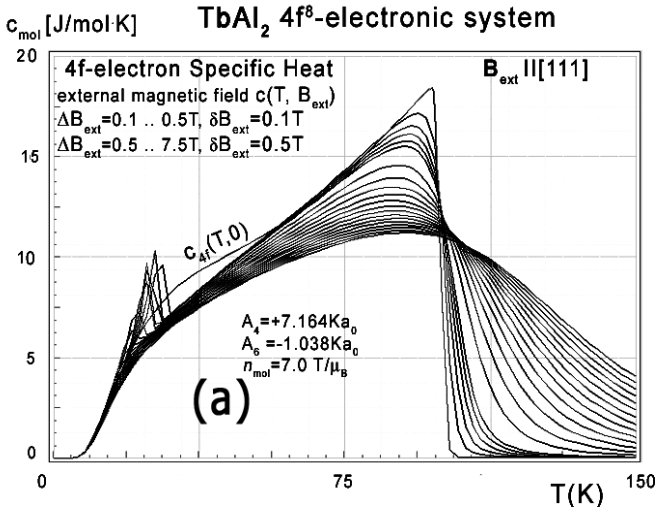

Preprints (www.preprints.org) | NOT PEER-REVIEWED | Posted: 14 June 2018 doi:10.20944/preprints201806.0236.v1

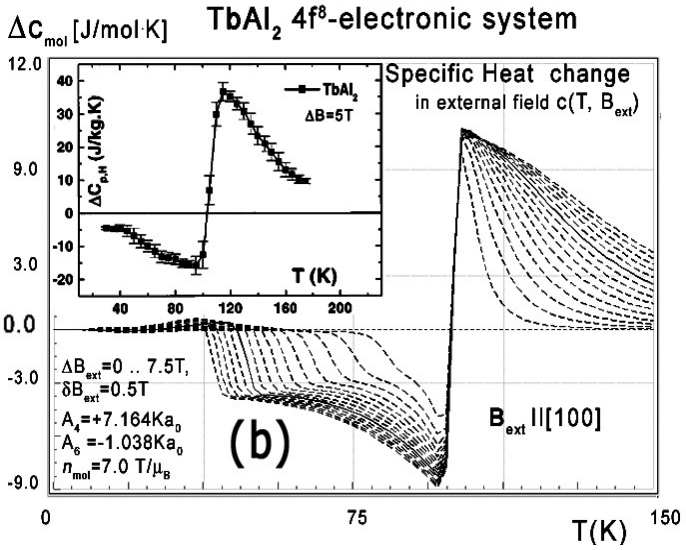

Fig. 46. (a) Calculated 4*f*-electron component of molar specific heat vs. temperature for Tb ions in $TbAl_2$ under the influence of an external magnetic field applied along [111] direction from 0 up to 7.5 T. **(b)** Calculated specific heat change vs. temperature for Tb ions in $TbAl_2$, under the influence of an external magnetic field applied along [100] direction from 0 to 7.5 T with step 0.5 T in comparison with experimental data from [5]. Solid line represents simulation for $\Delta B_{ext} = 0.5$ T.

Collected data of specific heat allows to calculate isothermal entropy change $-\Delta S(T,B_{ext})$ according to (16), the same methodology as used by experimentalists [3-7]. Isothermal entropy changes calculated with various external magnetic fields applied along all main directions of the cubic structure are presented in Fig. 47.

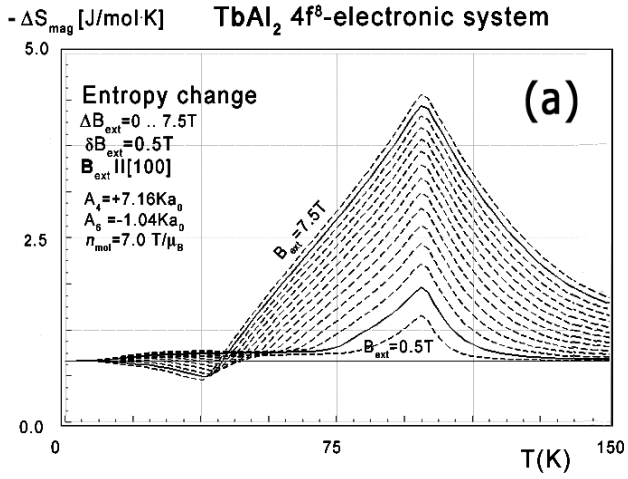

Preprints (www.preprints.org) | NOT PEER-REVIEWED | Posted: 14 June 2018 doi:10.20944/preprints201806.0236.v1

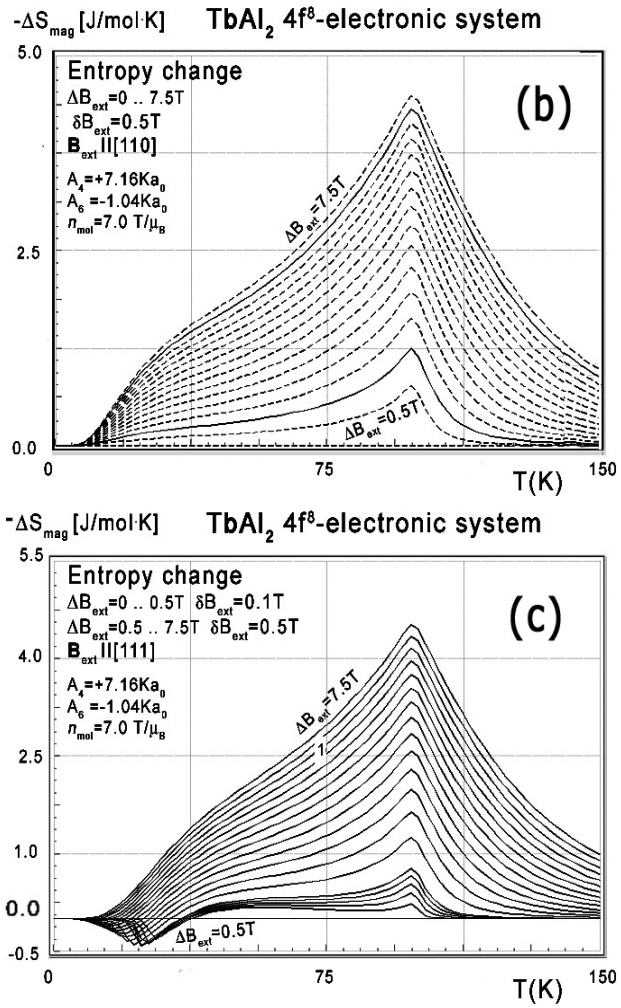

Fig. 47. Calculated isothermal entropy change of 4*f*-electronic system vs. temperature (16) of Tb ions in $TbAl_2$ under the influence of various external magnetic field values from 0 to 7.5 T with step 0.5 T **(a)** applied along [100] direction; **(b)** applied along [110] direction; **(c)** applied along [111] direction.

For the sake of completeness, calculations of magnetic moment vs. temperature under various external magnetic field conditions were also performed. The graphs of $\mathbf{m}(T,\mathbf{B}_{ext})$ are presented in Fig. 10. The simulated thermal evolution of magnetic moment components under the influence of external magnetic field along [110] direction shown in Fig. 48(b) clearly confirms [110] direction as an easy magnetization axis of $TbAl_2$. The applied external magnetic field along this direction confirms perfect parallel directions of magnetic vector and external magnetic field (note: in cubic symmetry [110] = [011] = [101]).

Preprints (www.preprints.org) | NOT PEER-REVIEWED | Posted: 14 June 2018 doi:10.20944/preprints201806.0236.v1

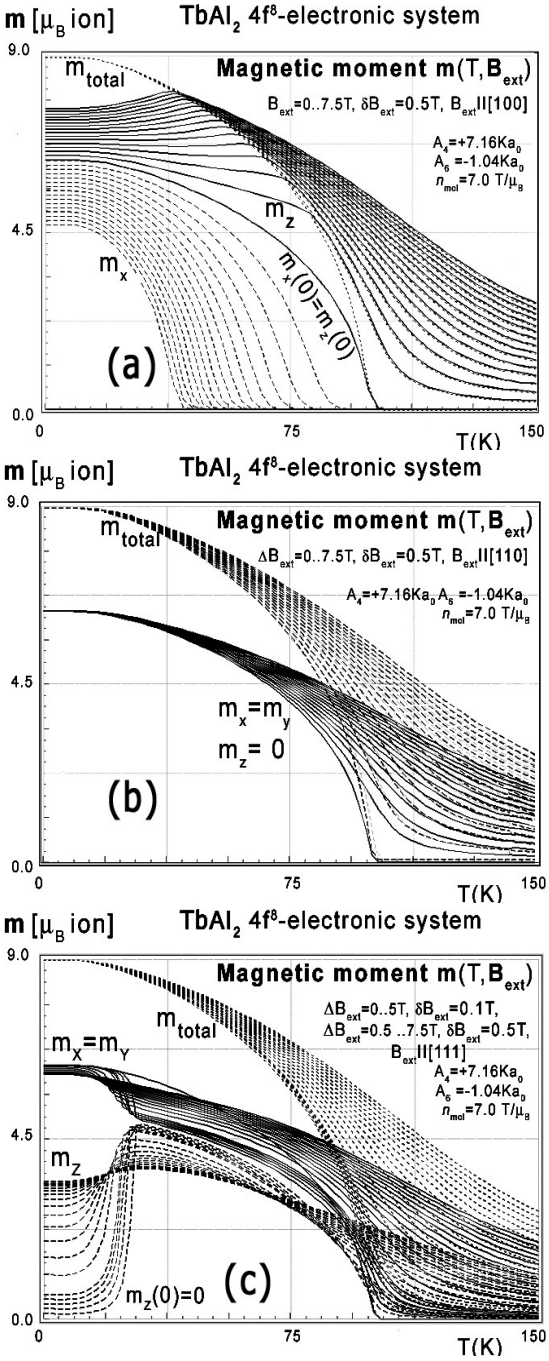

Fig. 48. Calculated x,y,z-directional components of total magnetic moment vs. temperature, calculated for Tb ions in $TbAl_2$ under the influence of CEF and molecular magnetic field and various values of external magnetic field from 0 to 7.5 T with step 0.5 T **(a)** applied along [100] direction; **(b)** applied along [110] direction; **(c)** applied along [111] direction.

Magnetic moment calculated in external magnetic field parallel to [111] and [100] direction reveals unusual behavior of the directional component of total moment. Similar behavior of magnetic moment directions was reported in [4], but most of the presented results of calculations of properties of $TbAl_2$ still await experimental verification. We found only a few reports about measurements of thermomagnetic properties of $TbAl_2$ single crystals. Some experimental comparative data of isothermal entropy change measured on $TbAl_2$ single crystals is provided by P.O. Ribeiro et al. [20],

Preprints (www.preprints.org) | NOT PEER-REVIEWED | Posted: 14 June 2018 doi:10.20944/preprints201806.0236.v1

and interesting specific heat change measured on polycrystalline sample is provided by F.W. Wang at al. [19]. All experimental data from [3-6] confirms the correctness of our approach in predicting the thermomagnetic properties of $TbAl_2$.

6.2 Calculated thermomagnetic properties of $SmAl_2$

In case of Sm^{3+} ions in $SmAl_2$, the spin and orbital magnetic moments of the magnetic ions under condition of defined CEF are found always antiparallel coupled and the magnitude of its orbital magnetic moment is always larger than that of the spin one. Calculations of electronic states in a paramagnetic state (ATOMIC MATTERS methodology) reveals this antiparallel coupling between spin and orbital momentum. The full structure of energy level in a paramagnetic state, calculated in $|L,S,L_z,S_z>$ space, together with expected values of angular momentum (spin and orbital) of particular states is shown in Fig. 49.

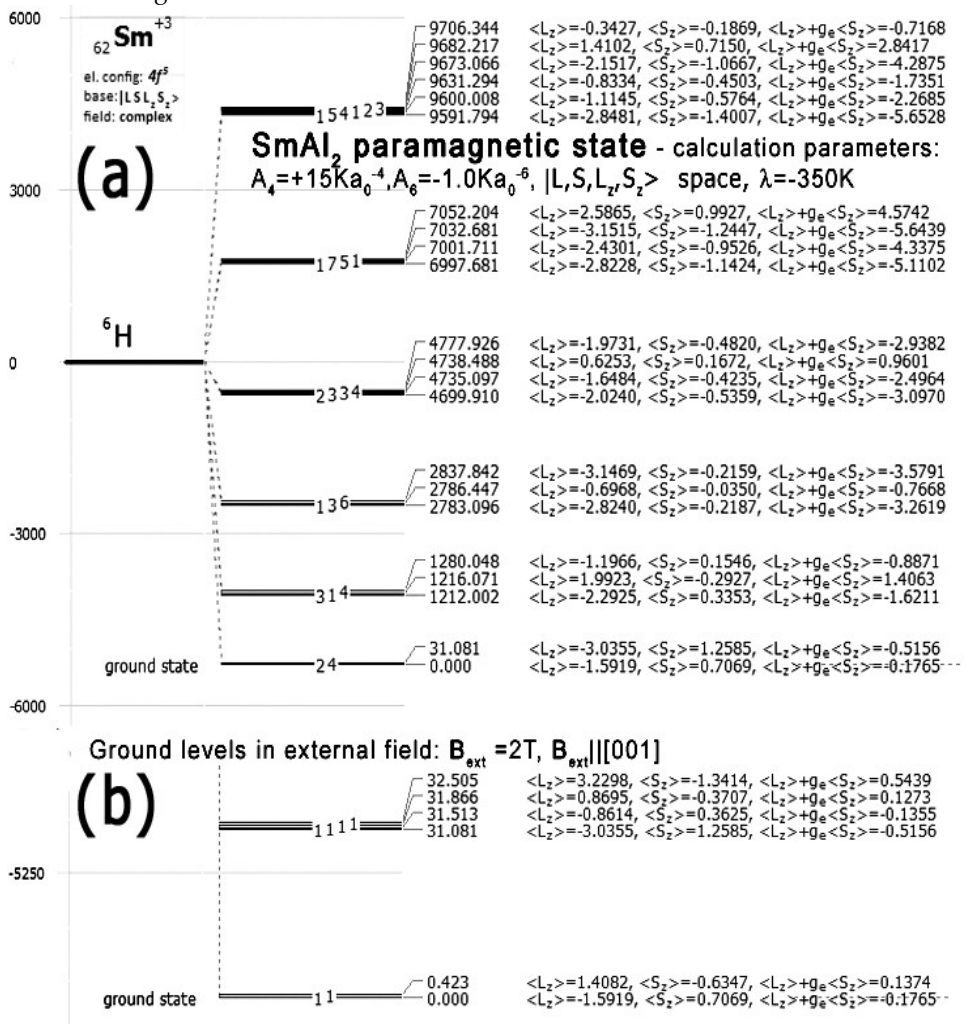

Preprints (www.preprints.org) | NOT PEER-REVIEWED | Posted: 14 June 2018 doi:10.20944/preprints201806.0236.v1

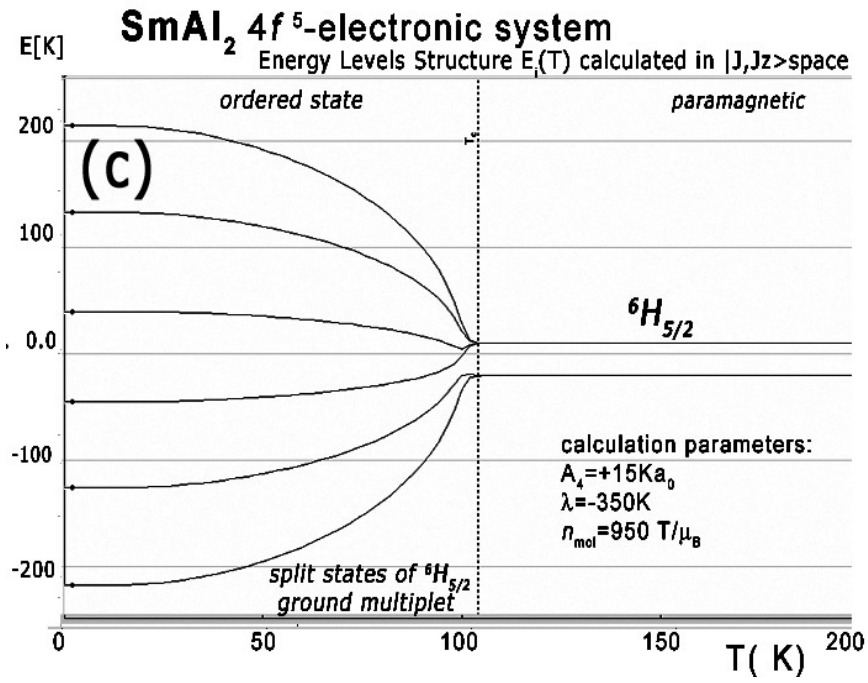

Fig. 49. (a) Energy level structure of Sm^{3+} ion $E_i(K)$ under the influence of defined CEF of $SmAl_2$ calculated in $|L,S,L_z,S_z>$ space. **(b)** Lowest state of this structure, calculated under the influence of external magnetic field $B_{ext} = 2$ T applied along [001]. **(c)** Ground multiplet energy level structure vs. temperature calculated for $4f^5$ electronic system of Sm^{3+} in $SmAl_2$ calculated in $|J,Jz>$ space.

The obtained electronic structure clearly demonstrates spin and orbital compensation of expected values of spin and orbital component of total angular momentum.

Calculations of energy level structure according to MFA methodology, in simplified $|J,Jz>$ space, according to (6) (ground J-multiplet only) provide primitive energy level structure shown in Fig. 15(c). According to the described methodology we calculated the total moment **m**(T) under the influence of molecular field (Fig. 50). To achieve Curie temperature T_C of about 120K, the value of the molecular field parameter was estimated at about $n_{mol} = 950T/\mu_B$. We do not have an explanation for such a large value of n_{mol}. The value of the ordered moment at T = 0K achieved that way is approx. $m(0) = 0.73\mu_B$, about four times higher than the experimental value $m_{exp} = 0.2\mu_B$ [17-22].

Preprints (www.preprints.org) | NOT PEER-REVIEWED | Posted: 14 June 2018 doi:10.20944/preprints201806.0236.v1

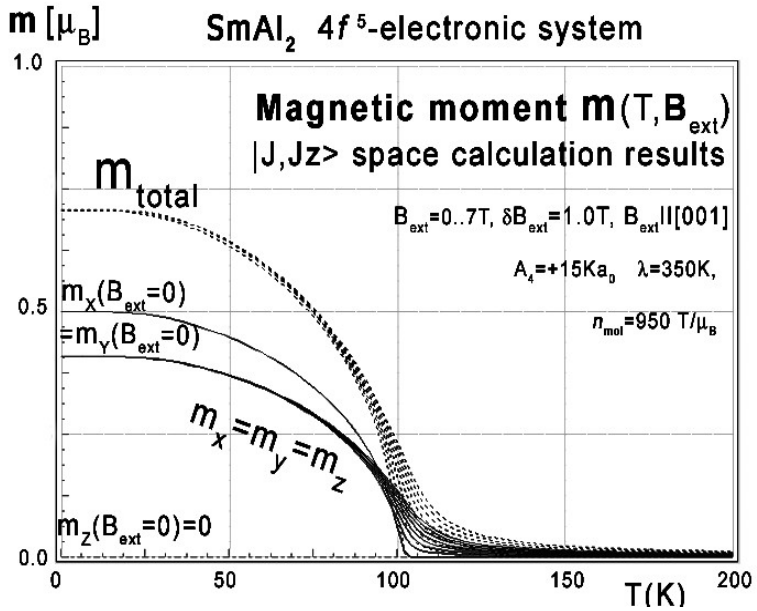

Fig. 50. Calculated x,y,z-directional components of total magnetic moment vs. temperature, calculated for $4f^5$ electronic system of Sm^{3+} in $SmAl_2$ calculated in |J,Jz> space.

The energy level structure makes it possible to calculate localized electron specific heat under the influence of an external magnetic field as shown in Fig. 51(a).

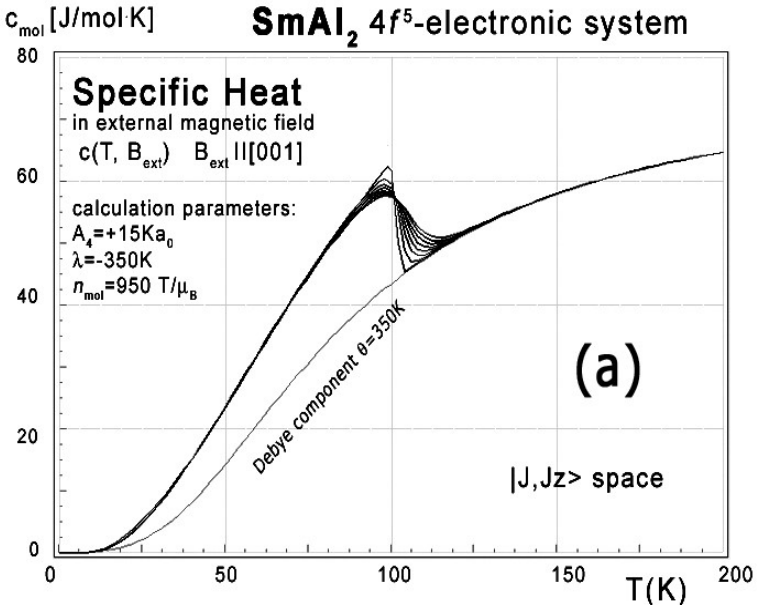

Preprints (www.preprints.org) | NOT PEER-REVIEWED | Posted: 14 June 2018 doi:10.20944/preprints201806.0236.v1

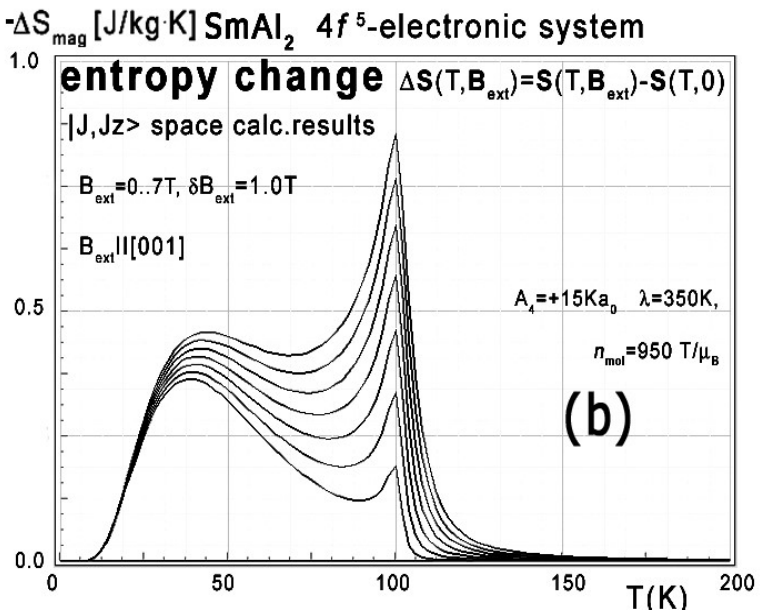

Fig. 51. (a) Calculated 4*f*-electron component of molar specific heat (14) with Debye crystal lattice component (θ = 350K) vs. temperature for Sm^{3+} ions in $SmAl_2$ under the influence of an external magnetic field applied along [001] direction. **(b)** Calculated isothermal entropy change of 4*f*-electronic system vs. temperature (16) of Sm^{3+} ions in $SmAl_2$ under the influence of an external magnetic field from 0 to 7 T applied along [001] direction

6.3. Calculated thermomagnetic properties of $GdAl_2$

The electronic configuration of Gd atoms consists of a closed shell inactive atomic core [$_{54}$Xe], a half filled 4*f* shell (e.g. electronic system $4f^7$), and outer electrons $5d^16s^2$. We attribute the magnetic properties of $GdAl_2$ compound to be an effect of properties of $4f^7$ electronic system under the influence of electromagnetic interactions defined according to the description in the theory section. The starting point of our analysis is the ground atomic term ^{8}S with the quantum number of orbital angular momentum L = 0 and total spin S = 7/2. This means Gd is a pure spin system. According to this, CEF does not interact with electronic states of the ground atomic term ^{8}S. In consequence, according to our approach, there is no source of single ionic anisotropy of Gd^{+3} ions with $4f^7$ electronic system. Inter-atomic magnetic interactions according to our MFA approach have pure isotropic nature (4) and (5), therefore the obtained properties of $GdAl_2$ are absolutely identical despite the direction of the magnetic field applied. The value of molecular field factor n_{mol} for $GdAl_2$ was established according to de Gennes scaling [10] $n_{mol}^{Gd} = 17.0T/\mu_B$. The calculated energy level structure is shown in Fig. 11(a).
In the absence of an external magnetic field, the ground term of the $4f^7$ electronic system is fully degenerated. A self-consistent molecular field splits these states at $T < T_C$. The value of the molecular field changes, and at T = 0 (absolute zero) $B_{mol} = 63$ T.

The calculations of electronic structure under the influence of an external magnetic field applied along [111] direction was also performed. The energy level structure calculated for the external magnetic field in this direction does not contain any anomalies. Specific heat calculated in this condition is shown in Fig. 52.

Preprints (www.preprints.org) | NOT PEER-REVIEWED | Posted: 14 June 2018 doi:10.20944/preprints201806.0236.v1

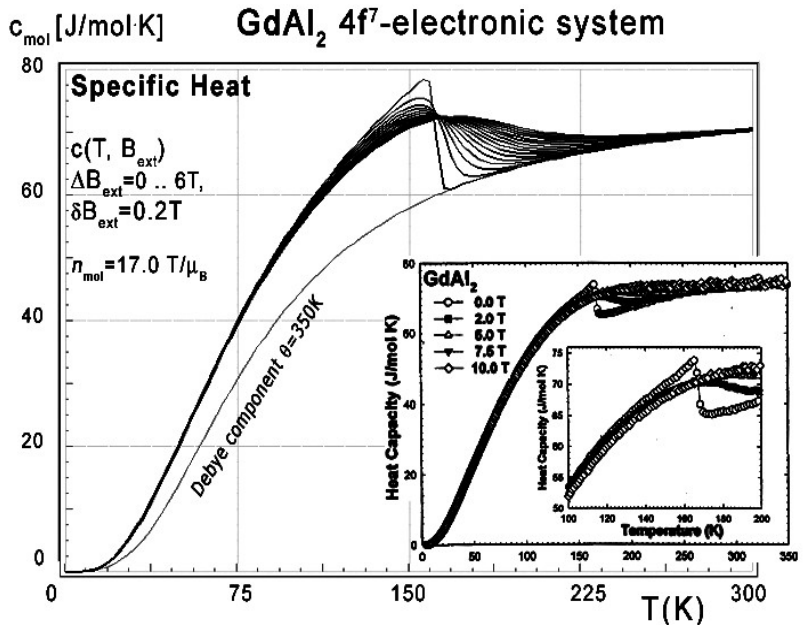

Fig. 52. Calculated 4*f*-electron component of molar specific heat (14) with Debye crystal lattice component (θ = 350K) vs. temperature of Gd ions in $GdAl_2$ under the influence of external magnetic field from 0 to 6 T with step 0.2 T. Inset: experimental data from [7]

Collected specific heat data makes it possible to calculate isothermal entropy change $-\Delta S(T,\mathbf{3})$ according to (16), the same methodology as used by experimentalists [3-7]. Isothermal isotropic entropy change calculated with various values of external magnetic field is presented in Fig. 53. The reference data taken from experimental measurement [3] is shown in the insets.

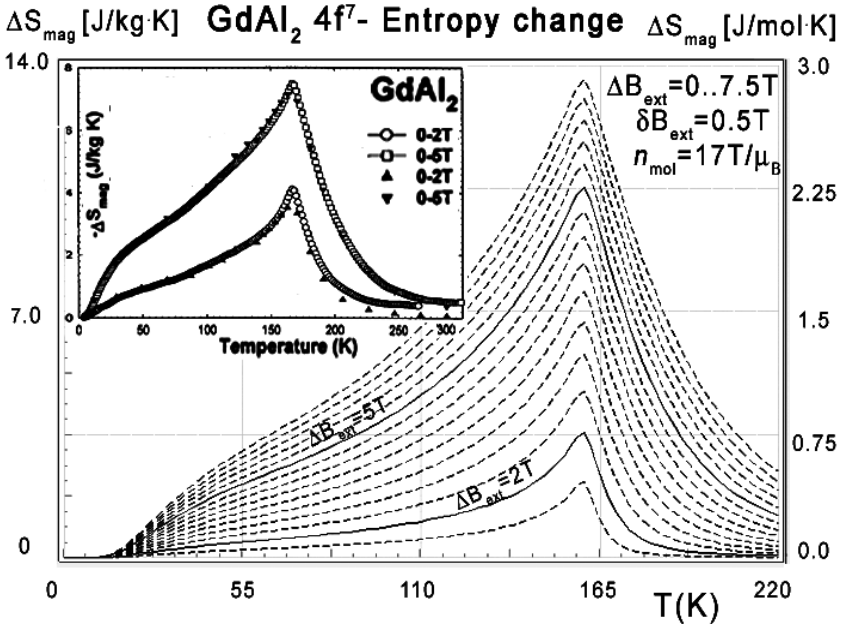

Fig. 53. Calculated isothermal entropy change of 4*f*-electronic system vs. temperature (16) of Gd ions in $GdAl_2$ under the influence of various values of external magnetic fields from 0 to 7.5 T with step 0.5 T. Inset: isothermal entropy change obtained from experimental data, taken from [7]. Experimental data shown in inset corresponds with calculated solid curves for $\Delta B_{ext} = 2$ T and $\Delta B_{ext} = 5$ T.

Preprints (www.preprints.org) | NOT PEER-REVIEWED | Posted: 14 June 2018 doi:10.20944/preprints201806.0236.v1

The isotropic behavior of calculated thermomagnetic properties agrees with experimental data [6, 7]. For completeness, magnetic moment calculations vs. temperature under various external magnetic field conditions were performed - the results are presented in Fig. 54.

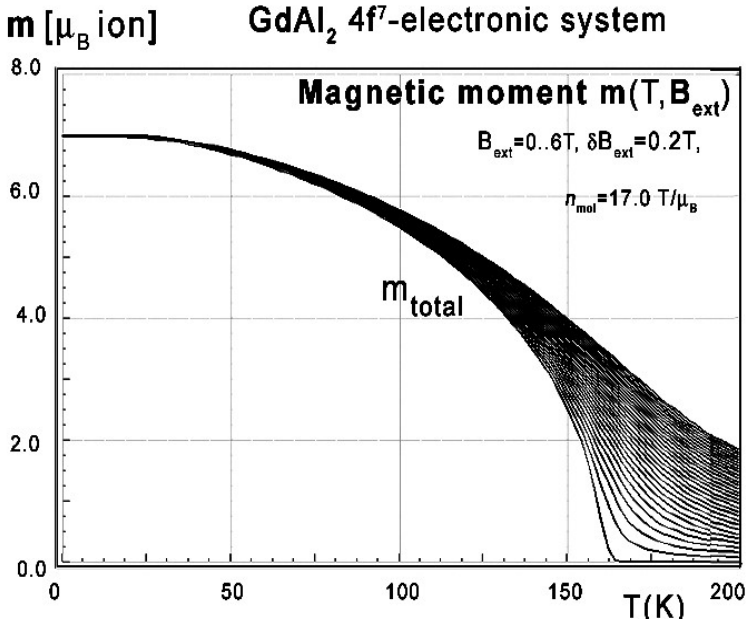

Fig. 54. Calculated unidirectional total magnetic moment vs. temperature, calculated for Gd ions in $GdAl_2$ under the influence of molecular magnetic field and various values of external magnetic field from 0 to 6.0 T with step 0.2 T.

7. Conclusions

In the first step we performed calculations of Dy^{3+} ions in the cubic CEF characteristic for Laves Phase C15 adequate for $ReAl_2$ crystals. Single-ionic thermomagnetic properties of $DyAl_2$ calculated with the ATOMIC MATTERS MFA computation system bases of the local symmetry of the Dy in the point symmetry for R ion is $\bar{4}3m$. The local symmetry of R ions in this structure is cubic, which significantly simplifies the analysis. All the calculations were performed with only 2 cubic CEF parameters and molecular field factor n_{mol}. The excellent agreement obtained between the calculated thermomagnetic properties and the reference data confirms the effectiveness of our theoretical approach.

Thermomagnetic properties of materials such as $\Delta S(T,\mathbf{B}_{ext})$ and $\mathbf{m}(T,\mathbf{B}_{ext})$ are currently an area of re-interest of researchers due to searching for effective materials for refrigerators working on the basis of magnetocaloric effect. As we have shown, magnetocaloric properties of materials can be well predicted based on the knowledge of the CEF crystalline field for paramagnetic ions (responsible for MCE) in the analyzed material. There is, however, not much information on the magnetocaloric properties of materials, even well-known and tested for other functional aspects. There is a huge knowledge base regarding crystalline fields of thousands of chemical compounds in solid state. Our application is able to convert parameters of CF, CEF, ZFS and LF models written in various conventions (Wybourne, Racach, Stevens) to the universal CEF convention in the A^{m}_{n} parameter language. Thanks to this, it is a tool that allows researchers to easily get knowledge about thermomagnetic properties of a material based on the methodology described in chapter 3, using the introduction of CEF coefficients to the software and allowing the researcher to select the convention. Recalculation of CEF coefficients between different compounds in the isostructural series leads to establishing a new set of crystal field parameters. With a significant confidence level we are able to predict properties of new materials, in particular their thermomagnetic behavior. The effectiveness of this methodology is confirmed by the presented calculation results for materials $DyAl_2$, $HoAl_2$,

$ErAl_2$, $TbAl_2$, $SmAl_2$ and $GdAl_2$. According to established universal CEF parameters (A^m_n) for all RAl_2 compounds, we performed similar calculations for $HoAl_2$ and $ErAl_2$ thermomagnetic properties. The local symmetry of the Ho and Er ions is cubic, which significantly simplifies the analyses. All the calculations were performed without free parameters. Very good agreement was obtained between thermomagnetic properties and experimental data confirms the effectiveness of our theoretical approach. Working with ATOMIC MATTERS MFA has revealed its high usefulness. The visual form of calculation results, full 3D interactive CEF potential visualization, intuitive tools for convention and unit recalculation, and the ability to compare data results all allow users to utilize the power of the application very effectively. In conclusion, we confirm that ATOMIC MATTERS MFA is a unique application that combines a package of tools for correctly describing the physical properties of atomic-like electron systems subjected to electromagnetic interactions in real materials. This is an accurate tool for calculating properties of ions under the influence of the electrostatic potential of definable symmetry and both external and inter-ionic magnetic fields taken as a mean field approximation in magnetically ordered state.

References

[1] Michalski R. and Zygadło J. (2016) Describing the Fine Electronic Structure and Predicting Properties of Materials with ATOMIC MATTERS Computation System *Proceedings: 18th Int. Conf. on Physics, Mathematics and Computer Science - Dubai UE* http://waset.org/publications/10004653/pdf

[2] Michalski R. and Zygadło J. (2016) Thermal dependences of single ionic, magnetic properties of materials in ordered state, calculated with ATOMIC MATTERS MFA computation system *Proceedings: 7th IIF-IIR International Conference on Magnetic Refrigeration at Room Temperature, Thermag VII - Torino ITALY*

[3] Lima A.L., Tsokol A.O., Gschneidner K.A. Jr, Pecharsky V.K., Lograsso T.A. and Schlagel D.L. (2005) *Phys. Rev. B* **72** 024403

[4] Purwins H.G. and Leson A. (1990) *Adv. Phys.* **39** 309

[5] Pecharsky V.K., Gschneidner K.A., Pecharsky A.O. and Tishin A.M. (2001) *Phys. Rev. B* **64** 144406

[6] von Ranke P.J., de Oliveira N.A., Plaza E.J.R., de Sousa V.S.R., Alho B.P., Magnus A., Carvalho G., Gama S. and Reis M.S. (2008) *Journal Of Applied Physics* **104** 093906

[7] Gil L.A., Campoy J.C.P., Plaza E.J.R. and de Souza M.V. (2016) *Journal of Magnetism and Magnetic Materials* **409** 45–49

[8] Patra M.S., Majumdar S., Giri S., Xiao Y. and Chatterji T. (2011) Magnetic and magnetoresistive properties of cubic Laves phase $HoAl_2$ single crystal *arXiv*:1107.1975 [cond-mat.mtrl-sci]

[9] Blaut A., Michalski R., Kocor M., Ropka Z., Baran A.J. and Radwanski R.J. (2003) *Acta Physica Polonica B* **34** 1261-1264

[10] Software website: www.atomicmatters.eu

[11] Rudowicz C. and Chung C.Y. (2004) The generalization of the extended Stevens operators *J. Phys.: Condens. Matter* **16** 5825–5847

[12] Hutchings M.T. (1964) *Solid State Phys.* **16** New York

[13] Franse J.J.M. and Radwanski R.J. (1993) Magnetic properties of binary rare-earth in *Handbook of Magnetic Materials* Vol **7**. ed. Bushow K.H.J. 307-500

[14] Radwański R.J., Michalski R., Ropka Z. and Blaut A. (2002) *Physica B* **319** 78–89

 doi:10.20944/preprints201806.0236.v1

[15] Szpunart B. and Lindgard P.A. (1979) *J. Phys. F: Metal Phys.* Vol. **9** No. 3

[16] de Gennes P.G. (1962) *J. Phys. Radiat.* **23** 5010

[17] Wybourne B.G. (1970) *Symmetry Principles and Atomic Spectroscopy* J. Wiley and Sons New York

[18] Abragam A. and Bleaney B. (1970) *EPR of Transition Ions*, Clarendon Press, Oxford

[19] Wang F.W., Zhang X.X. and Hu F.X. (2000) *Appl. Phys. Lett.* Vol. **77** No. 9 1360

[20] Ribeiro P.O., Alho B.P., Alvarenga T.S.T., Nóbrega E.P., deSousa V.S.R., Magnus A., Carvalho G., Caldas A., deOliveira N.A. and von Ranke P.J. (2015) *Journal of Magn. Magn. Mater.* **379** 112–116

[21] Wikusa P., Canavan E., Heine S.T., Matsumoto K. and Numazawa T. (2014) *Cryogenics Preprint*

[22] Michalski R. and Zygadło J. Predictions of thermomagnetic properties of Laves Phase compounds: $TbAl_2$, $GdAl_2$ and $SmAl_2$ performed with ATOMIC MATTERS MFA Computation System. *Journal of Magnetism and Magnetic Materials* 452 (2018) 415–426.